NACA

RESEARCH MEMORANDUM

EXPERIMENTAL DOWNWASH AND WAKE CHARACTERISTICS AT SUBSONIC AND SUPERSONIC MACH NUMBERS BEHIND AN UNSWEPT, TAPERED WING OF ASPECT RATIO 2.67 WITH LEADING- AND TRAILING-EDGE FLAPS

By Harold J. Walker, Louis S. Stivers, Jr.,
and Luther Beard, Jr.

Ames Aeronautical Laboratory
Moffett Field, Calif.

NATIONAL ADVISORY COMMITTEE
FOR AERONAUTICS

WASHINGTON
April 20, 1951

NATIONAL ADVISORY COMMITTEE FOR AERONAUTICS

RESEARCH MEMORANDUM

EXPERIMENTAL DOWNWASH AND WAKE CHARACTERISTICS AT SUBSONIC AND SUPERSONIC MACH NUMBERS BEHIND AN UNSWEPT, TAPERED WING OF ASPECT RATIO 2.67 WITH LEADING- AND TRAILING-EDGE FLAPS

By Harold J. Walker, Louis S. Stivers, Jr.,
and Luther Beard, Jr.

SUMMARY

The effect of Mach number on the characteristics of the downwash and wake behind an unswept, tapered wing of aspect ratio 2.67 with full-span, 25-percent-chord, leading- and trailing-edge flaps has been determined from wind-tunnel tests. The wing section was uniformly 8-percent chord thick between the 25- and 75-percent-chord points, and tapered to sharp leading and trailing edges. The results are presented for Mach numbers between 0.50 and 0.95 and between 1.09 and 1.29 with ranges of leading-edge flap deflection from -20° to 10° and of trailing-edge flap deflection from 0° to 40°. The Reynolds numbers, based on the mean aerodynamic chord, varied from 0.94×10^6 to 1.27×10^6. The downwash angles at the 25-, 50-, and 62.5-percent-semispan stations were measured for angles of attack between -12° and 12° at a distance of 1.80 mean aerodynamic chord lengths downstream from the midchord line of the wing. The location and thickness of the wake at the 50-percent-semispan station were measured for angles of attack between -7.4° and 13.0° at a distance of 4.74 mean aerodynamic chord lengths downstream from the midchord line of the wing.

In general, the variation of downwash angle with angle of attack was not significantly affected by Mach number. In the Mach number ranges investigated, differences in the rates of change of downwash angle with lift coefficient (at zero angle of attack) for the various combinations of flap deflection were found which are believed to be due principally to differences in spanwise load distribution. For the wing with undeflected flaps, the calculated values of the rates of change of downwash angle with lift coefficient appeared to be in accord with the trend of the experimental values at the subsonic Mach numbers.

The effects of Mach number, angle of attack, and flap deflection on the wake thickness were, in general, those that would normally be

expected. The variation of wake location with angle of attack was nonlinear for the configurations involving large flap deflections, and was essentially independent of Mach number. For the wing with undeflected flaps, the experimental and calculated locations of the wake (vortex sheet) expressed as a function of lift coefficient were in reasonable agreement.

INTRODUCTION

Previous investigations of the downwash and wake behind lifting surfaces at subsonic and supersonic Mach numbers have been concerned largely with wings having no control surfaces, although some attention has been given to the effects of trailing-edge flap deflection in the investigations reported in references 1 and 2. The results presented in these references, however, are only for high-aspect-ratio wings at low speed. In general, little is known of the effects of control-surface deflection at high subsonic and at supersonic Mach numbers.

The present investigation was undertaken in the Ames 1- by 3-1/2-foot high-speed wind tunnel to provide some experimental evidence of the effects of leading- and trailing-edge flap deflections on the characteristics of the downwash and wake behind a low-aspect-ratio wing at subsonic and supersonic Mach numbers. In this investigation, measurements have been made of the downwash angles at three spanwise stations and of the location and thickness of the wake at one spanwise station behind a semispan model for various angles of attack and combinations of flap deflections. Comparisons between the experimental and calculated effects of Mach number on these characteristics are included for the case of undeflected flaps.

SYMBOLS

c	chord length of wing section
$\bar{c}$	wing mean aerodynamic chord length $\left(\frac{\int c^2 dy}{\int c\ dy}\right)$
C_L	lift coefficient $\left(\frac{\text{lift}}{qS}\right)$
M	Mach number
q	free-stream dynamic pressure

[redacted]

R Reynolds number based on mean aerodynamic chord

s wing semispan

S wing area

t wing thickness

x,y,z Cartesian coordinates in the longitudinal, lateral, and vertical directions, respectively, with the origin at the quarter-chord point of the mean aerodynamic chord, and with the x axis coinciding with the line of intersection of the plane of the wing and the vertical plane of symmetry

α wing angle of attack, degrees

ϵ downwash angle measured with respect to the free-stream direction, degrees

δ_f trailing-edge flap deflection, measured in a plane normal to the hinge line (positive when the trailing edge is below the chord plane), degrees

δ_n leading-edge flap deflection, measured in a plane normal to the hinge line (positive when the leading edge is above the chord plane), degrees

δ_M jet-boundary correction factor to the downwash angle

APPARATUS

The tests were conducted in the Ames 1- by 3-1/2-foot high-speed wind tunnel, which was equipped with a flexible throat to permit operation at both subsonic and supersonic Mach numbers.

A semispan model of a wing having an aspect ratio of 2.67, a taper ratio of 0.5, and an unswept 50-percent-chord line was used in the investigation. The wing sections were symmetrical and tapered from a thickness of 8 percent of the chord between the 25- and 75-percent-chord points to sharp leading and trailing edges. The wing was equipped with full-span, 25-percent-chord, plain, leading- and trailing-edge flaps having hinge lines which coincided with the 25- and 75-percent-chord lines. The model was constructed of steel to the dimensions shown in figure 1, and its surfaces were ground and polished. The leading- and trailing-edge radii were approximately 0.002 inch.

[redacted]

A circular plate mounted flush with the tunnel wall (fig. 2) served as a support for both the model and the apparatus for measuring the downwash angles. The angle of attack of the model was varied by rotating the entire plate assembly.

The downwash angles were measured by means of the small probe illustrated in figure 1. The head of the probe was hemispherical and contained two orifices located symmetrically with respect to the probe axis in a vertical plane through this axis. The downwash angle relative to the free-stream direction was determined by pitching the probe to the angle at which the pressure difference between the orifices was zero. The downwash angles could be measured to the nearest 0.1° by means of this probe. Total-pressure surveys of the wake from the model were made with a rake consisting of fifty 1/16-inch-diameter tubes spaced at quarter-inch intervals. (See fig. 2.)

TESTS

Downwash angles were measured at the 25-, 50-, and 62.5-percent-semispan stations at a distance of 1.80 mean aerodynamic chord lengths downstream from the midchord line of the wing and 0.51 mean aerodynamic chord lengths above the extended chord plane of the wing (fig. 1) at angles of attack from −12° to 12° and at Mach numbers from 0.50 to 0.95 and from 1.09 to 1.29 for the following combinations of leading- and trailing-edge flap deflections:

δ_n, degrees	δ_f, degrees
0	0
−10	0
10	0
0	20
10	20

At Mach numbers near unity, the range of angle of attack was limited by wind-tunnel choking. Satisfactory measurements of the downwash angles could not be made at the angles of attack for which the probe was located in the turbulent flow in the region of the wake. For these tests, the Reynolds numbers, based on the mean aerodynamic chord, varied from about 0.94×10^6 to 1.27×10^6, as shown in figure 3.

The investigation of the wake, which was made independently of that of the downwash, included measurements at several angles of attack between −7.4° and 13.0° of the locations of the boundaries of the wake and of the point of maximum total-pressure defect, but not of the

[redacted]

magnitudes of the pressure defects. The wake measurements were determined at the 50-percent-semispan station at a distance of 4.74 mean aerodynamic chord lengths downstream from the midchord line of the wing at Mach numbers from 0.50 to 0.85 and at 1.20 and 1.29 for the following combinations of flap deflections:

δ_n, degrees	δ_f, degrees
0	0
10	0
0	20
10	20
-10	20
-20	40

All the tests were made with the gaps between the wing and the flaps unsealed.

CORRECTIONS TO DATA

Stream-angle surveys with the model removed from the tunnel were made in a vertical plane at each spanwise station for the range of Mach numbers investigated. The stream angles, which were generally less than $\pm 0.3^\circ$, were applied as corrections to the measured downwash angles.

The geometric angles of attack were corrected for the effects of the tunnel walls at subsonic Mach numbers by the method of reference 3. The correction, which is shown in reference 4 to be independent of Mach number, is given by the expression

$$\Delta\alpha = 0.51\ C_L$$

Corrections for the tunnel-wall effects at subsonic Mach numbers were applied to the measured downwash angles according to the method of reference 5. This correction reduces to the expression

$$\Delta\epsilon = 2.24\ \delta_M C_L$$

in which the factor δ_M was determined for an elliptic spanwise loading on a 5-inch-semispan lifting line located in the center of the 3-1/2-foot dimension of the tunnel. Values of δ_M corresponding to the various subsonic Mach numbers were determined from figure 4 of reference 6.

[redacted]

RESULTS AND DISCUSSION

Downwash Characteristics

Variation of downwash angle with angle of attack.— The variations of the downwash angle with angle of attack for the various combinations of leading- and trailing-edge flap deflections are presented in figures 4, 5, and 6 for the 25-, 50-, and 62.5-percent-semispan stations, respectively. The increase in the slopes of the curves with increase in angle of attack, evident in these figures, is characteristic of downwash measurements made at a point situated above the wake at a fixed distance from the wing chord plane, and is due to the decrease in the distance between this point and the wake as the angle of attack is increased.

The irregularities appearing in some of the curves of figures 4, 5, and 6, notably those corresponding to the leading-edge flap deflection of -10° and to several of the supersonic Mach numbers, cannot be satisfactorily explained on the basis of the available data. The influence of the wake and the effects of shock waves may have been contributing factors. The failure of the curves for the case of undeflected flaps to pass through the origin at the higher Mach numbers may possibly be attributed to undetermined local stream angularities due to the presence of the model and to small misalinements of the flaps. It would be expected that these same effects influenced the downwash characteristics behind the wing with the various combinations of flap deflections.

Rate of change of downwash angle with angle of attack.— The effect of Mach number on the rate of change of downwash angle with angle of attack at zero angle of attack (i.e., $(d\epsilon/d\alpha)_{\alpha=0}$) is shown in figure 7 for each of the curves presented in figures 4, 5, and 6. It is observed in figure 7 that the effects of Mach number on $(d\epsilon/d\alpha)_{\alpha=0}$ corresponding to the various flap deflections differ considerably at Mach numbers greater than about 0.8. The differences are believed to be due principally to the previously noted irregularities in the variation of downwash angle with angle of attack.

Since the downwash is directly related to the lift of the wing, some similarity would be expected between the effects of Mach number on $(d\epsilon/d\alpha)_{\alpha=0}$ (fig. 7) and $(dC_L/d\alpha)_{\alpha=0}$. Values of $(dC_L/d\alpha)_{\alpha=0}$ for the several combinations of flap deflections were determined from the data of references 7, 8, and 9 (obtained from tests of the wing model of the present investigation) and are presented in figure 8 as a function of Mach number. Calculated lift-curve slopes are also included in figure 8, but only for the wing with undeflected flaps. A comparison of figures 7 and 8 reveals that the expected similarity is evident at the subsonic Mach numbers below 0.8 for each combination of flap deflections, and at the supersonic Mach numbers only for the case of undeflected flaps.

[redacted]

The effect of flap deflection on the rate of change of downwash angle would be expected to be less pronounced if expressed in terms of lift coefficient rather than angle of attack. Curves of $(d\epsilon/dC_L)_{\alpha=0}$ as a function of Mach number therefore were determined from figures 7 and 8, and are presented in figure 9. The spread of the curves in figure 9 is believed to be due largely to differences in the spanwise load distributions for the several combinations of flap deflections.

The spanwise variation of $(d\epsilon/dC_L)_{\alpha=0}$ for Mach numbers of 0.50 and 0.80 is shown in figure 10. The rapid reduction in the outboard direction of the values for the case of negative leading-edge flap deflection would indicate that the spanwise loading for this case was largely concentrated near the vertical plane of symmetry.

Values of $(d\epsilon/dC_L)_{\alpha=0}$ in the vertical plane of symmetry of the wing were calculated for the wing with undeflected flaps and are compared in figure 11 with the corresponding experimental values between the 25- and 62.5-percent-semispan stations for Mach numbers of 0.50, 0.70, 0.80, 0.90, and 1.25. The calculations for the subsonic Mach numbers were determined by the lifting-line method of reference 1, assuming the spanwise load distribution on the wing to be elliptical. This spanwise loading was approximated by superposing five unswept U-vortices at the location of the quarter-chord point of the mean aerodynamic chord. The effects of compressibility were included using the relations for linearized compressible flow. The calculation for the supersonic Mach number was made by the lifting-line method of reference 10. The calculated values of $(d\epsilon/dC_L)_{\alpha=0}$ appear to be in accord with the trend of the experimental values except at the supersonic Mach number, for which the actual spanwise load distribution is believed to have differed considerably from the assumed elliptic distribution.

Wake Characteristics

The positions of the boundaries of the wake and of the point of maximum total-pressure defect at the 50-percent-semispan station at a distance of 4.74 mean aerodynamic chord lengths downstream from the midchord line of the wing are presented in figure 12 for the various combinations of leading- and trailing-edge flap deflections. The locations of the boundaries of the wake and of the point of maximum total-pressure defect above the extended chord plane of the wing are shown for angles of attack ranging from -7.4° to 13° and for Mach numbers between 0.50 and 0.85 and at 1.20 and 1.29.

It is noted in figure 12 that, except at the supersonic Mach numbers for the wing at the highest angles of attack, the point of maximum total-pressure defect lies approximately midway between the boundaries of the

wake. The asymmetry of the wake boundaries at the supersonic Mach numbers is believed to be the result of combined effects of shock waves and boundary-layer separation on the wing. The variations of wake thickness accompanying changes in Mach number, angle of attack, and flap deflection are such as would normally be anticipated on the basis of the corresponding drag characteristics. (See references 7, 8, and 9.)

A discussion of the location of the wake is facilitated by means of figure 13 in which the variation of the location of the point of maximum total-pressure defect with angle of attack is shown for the various combinations of flap deflections at several Mach numbers. The locations are seen to be essentially independent of Mach number except in the cases of positive leading-edge flap deflection at a Mach number of 1.29 (indicated by broken lines). The nondependence of wake location on Mach number has been observed experimentally in the investigation reported in reference 6, in which the wake characteristics were determined behind a triangular wing without flaps. It is also evident in figure 13 that the effect of angle of attack on the location of the wake is nonlinear for the combinations involving large deflections of the flaps.

In figure 13, an abrupt upward displacement of the point of maximum total-pressure defect is noted at the highest angles of attack for the wing with undeflected flaps. This upward displacement, as explained in reference 6, is believed to correspond to the appearance, at these high angles of attack, of the rolled-up portion of the wake in the vicinity of the plane of the survey rake as a result of an increase in the part of the spanwise load carried near the vertical plane of symmetry. Evidence of the rolled-up portion of the wake is not apparent in the data for the wing with deflected flaps.

The location of the points of maximum total-pressure defect (vortex sheet) with respect to the extended chord plane of the wing for the case of the undeflected flaps is shown in figure 14 as a function of lift coefficient. Calculated vertical locations of the vortex sheet at the 50-percent-semispan station and of the center of the tip-vortex core were determined from references 11 and 12 for an assumed elliptical spanwise loading, and are also included in this figure. The locations, when calculated with respect to the extended chord plane of the wing, depend on the angle of attack, which, since the lift curves corresponding to the various combinations of flap deflections were essentially linear (reference 7), can be more conveniently expressed in terms of the lift-curve slope. Experimental rather than calculated lift-curve slopes were employed in order to eliminate the influence of the known differences in these slopes in a comparison of the calculated and experimental wake locations. Rather than present the calculated locations of the vortex sheet and tip-vortex core for each Mach number, regions are shown having boundaries which were determined by the maximum and minimum slopes

given in figure 8 (viz., 0.0432 and 0.0536 corresponding to Mach numbers of 0.50 and 1.09, respectively, for the wing with undeflected flaps).

It is observed in figure 14 that the experimental points for lift coefficients less than about 0.2 lie below the calculated region, and thus indicate that the vortex sheet was located below the extended chord plane of the wing at zero lift. (See also fig. 13). This effect is believed to have been due to misalinement of the flaps. If the downward displacement of the experimental points in figure 13 were taken into account, the agreement between the experimental and calculated wake locations would be considered satisfactory. It is seen in figure 14 that at the highest lift coefficients only the experimental points for the lower Mach numbers lie within or near the calculated region for the tip-vortex core.

CONCLUDING REMARKS

The present investigation employing a wing of aspect ratio 2.67 with leading- and trailing-edge flaps reveals that, in general, there are no marked effects of Mach number on the variation of downwash angle with angle of attack for the various combinations of flap deflections at a distance of 1.80 mean aerodynamic chord lengths downstream from the midchord line of the wing. In the range of Mach numbers investigated, the rates of change of downwash angle with lift coefficient (at zero angle of attack) differ for the various flap deflections due, it is believed, to differences in spanwise load distribution. For the wing with undeflected flaps, the calculated values of the rates of change of downwash angle with lift coefficient appear to be in accord with the trend of the experimental values, except at the supersonic Mach number at which the comparison was made. The actual spanwise load distribution at this supersonic Mach number is believed to have differed considerably from the assumed elliptic distribution.

The effects of Mach number, angle of attack, and flap deflection on the wake thickness at the 50-percent-semispan station at a distance of 4.74 mean aerodynamic chord lengths downstream from the midchord line of the wing are generally consistent with those that might be anticipated. Except for the cases of positive leading-edge flap deflection at a Mach number of 1.29, the location of the wake is essentially independent of Mach number. The variation of wake location with angle of attack is nonlinear for the configurations involving large deflections of the flaps. For the wing with undeflected flaps, the experimental and calculated locations of the wake (vortex sheet) expressed as a function of

[redacted]

lift coefficient are in reasonable agreement except at several of the highest lift coefficients.

Ames Aeronautical Laboratory,
National Advisory Committee for Aeronautics,
Moffett Field, Calif.

REFERENCES

1. Silverstein, Abe, and Katzoff, S.: Design Charts for Predicting Downwash Angles and Wake Characteristics Behind Plain and Flapped Wings. NACA Rep. 648, 1939.

2. Silverstein, Abe, Katzoff, S., and Bullivant, W. Kenneth: Downwash and Wake Behind Plain and Flapped Airfoils. NACA Rep. 651, 1939.

3. Glauert, H.: Wind-Tunnel Interference of Wings, Bodies, and Airscrews. R.& M. No. 1566, British, Sept., 1933.

4. Goldstein, S., and Young, A. D.: The Linear Perturbation Theory of Compressible Flow with Applications to Wind-Tunnel Interference. R.& M. No. 1909, British, July, 1943.

5. Swanson, Robert S., and Schuldenfrei, Marvin J.: Jet-Boundary Corrections to the Downwash Behind Powered Models in Rectangular Wind Tunnels with Numerical Values for 7- by 10-Foot Closed Wind Tunnels. NACA ARR 119, 1942.

6. Walker, Harold J., and Stivers, Louis S., Jr.: Investigation of the Downwash and Wake Behind a Triangular Wing of Aspect Ratio 4 at Subsonic and Supersonic Mach Numbers. NACA RM A50I14a, 1950.

7. Stivers, Louis S., and Malick, Alexander W.: Wind-Tunnel Investigation at Mach Numbers from 0.50 to 1.29 of an Unswept Tapered Wing of Aspect Ratio 2.67 With Leading- and Trailing-Edge Flaps - Trailing-Edge Flaps Deflected. NACA RM A50J09b, 1950.

8. Stivers, Louis S., Jr., and Malick, Alexander W.: Wind-Tunnel Investigation at Mach Numbers from 0.50 to 1.29 of an Unswept Tapered Wing of Aspect Ratio 2.67 With Leading- and Trailing-Edge Flaps - Leading-Edge Flaps Deflected. NACA RM A50K10, 1950.

9. Stivers, Louis S., Jr., and Malick, Alexander W.: Wind-Tunnel Investigation at Mach Numbers from 0.50 to 1.29 of an Unswept Tapered Wing of Aspect Ratio 2.67 With Leading- and Trailing-Edge Flaps - Flaps Deflected in Combination. NACA RM A50K27b, 1950.

[redacted]

10. Mirels, Harold, and Haefeli, Rudolph C.: Line-Vortex Theory for Calculation of Supersonic Downwash. NACA TN 1925, 1949.

11. Spreiter, John R., and Sacks, Alvin H.: Rolling Up of the Trailing Vortex Sheet and Its Effect on the Downwash Behind Wings. Jour. Aero. Sci., January, 1951, pp. 21-32.

12. Westwater, F. L.: The Rolling Up of the Surface of Discontinuity Behind an Aerofoil of Finite Span. R.& M. No. 1692, British, 1936.

[redacted]

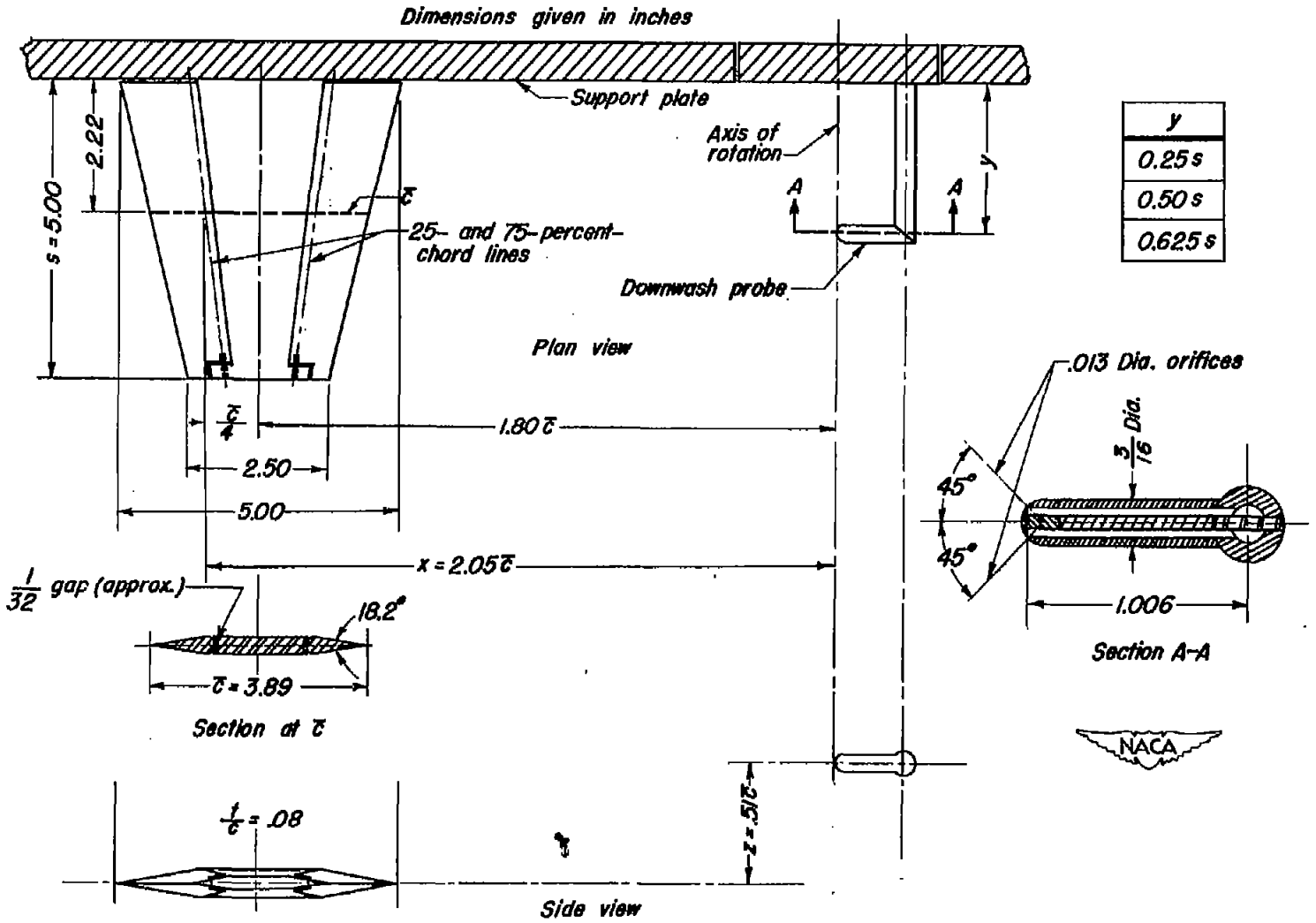

Figure 1.— Sketch of model and downwash probe, showing locations of downwash survey stations.

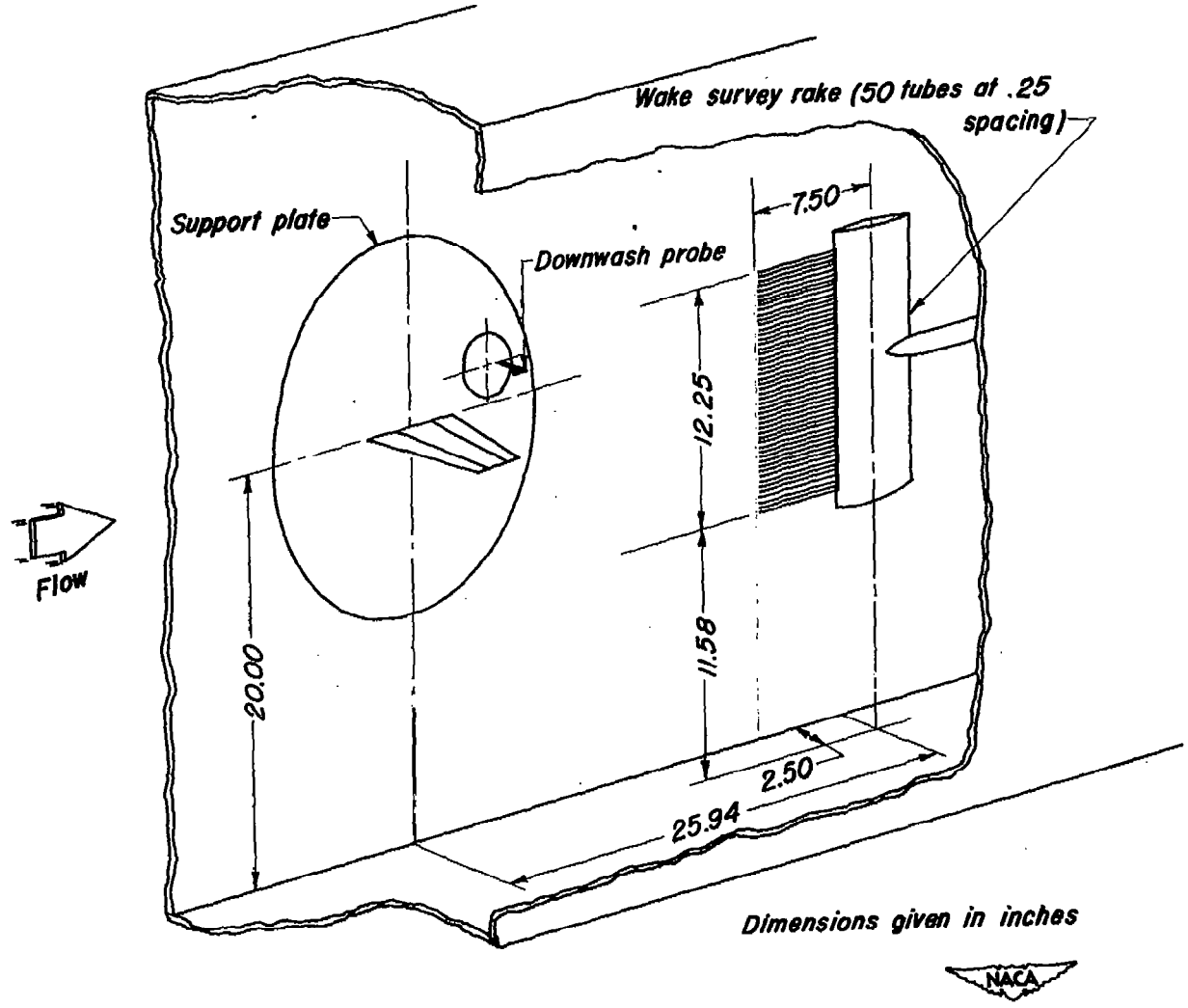

Figure 2.– Sketch of model support showing location of survey rake.

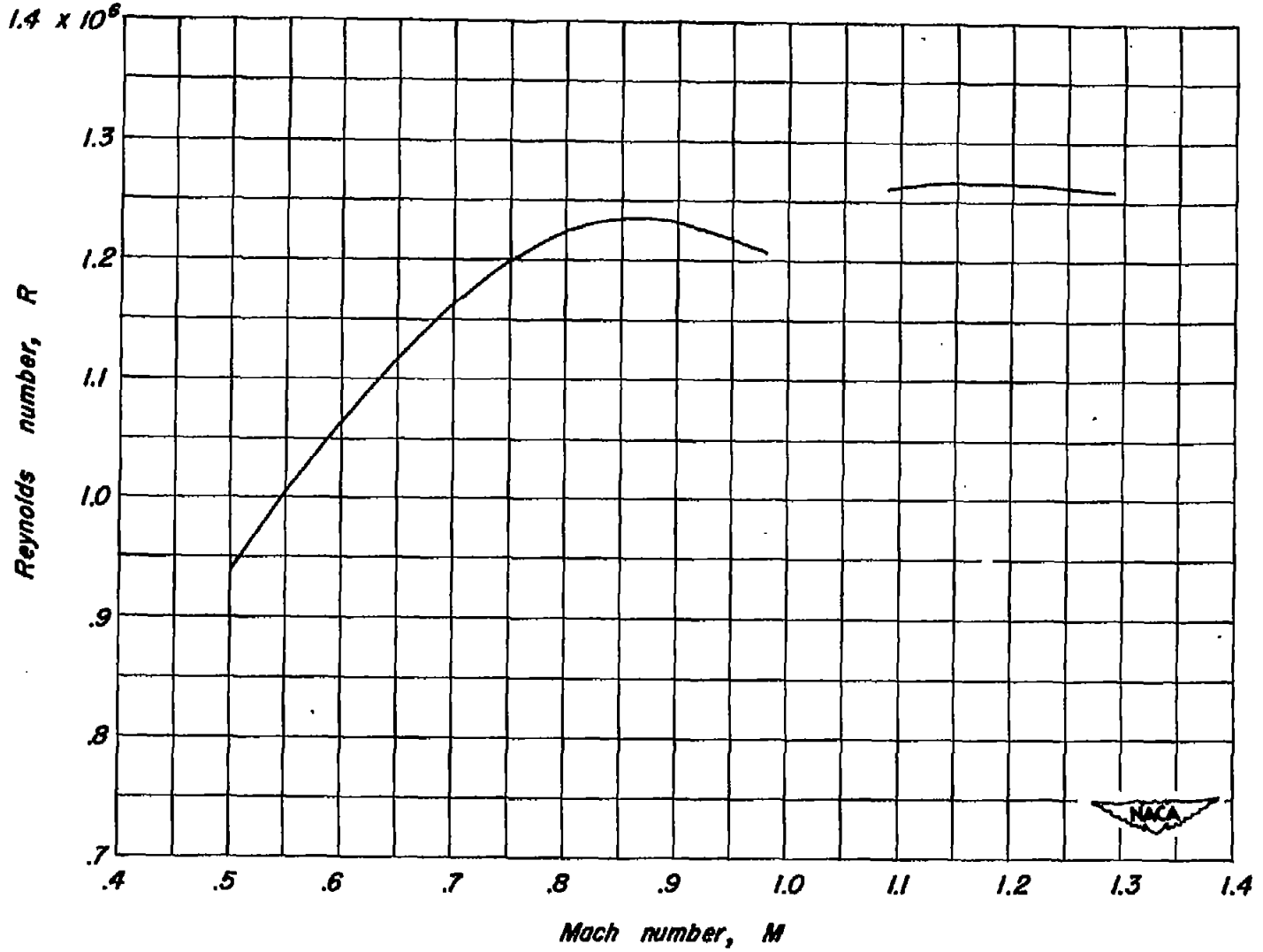

Figure 3.— Variation of Reynolds number with Mach number.

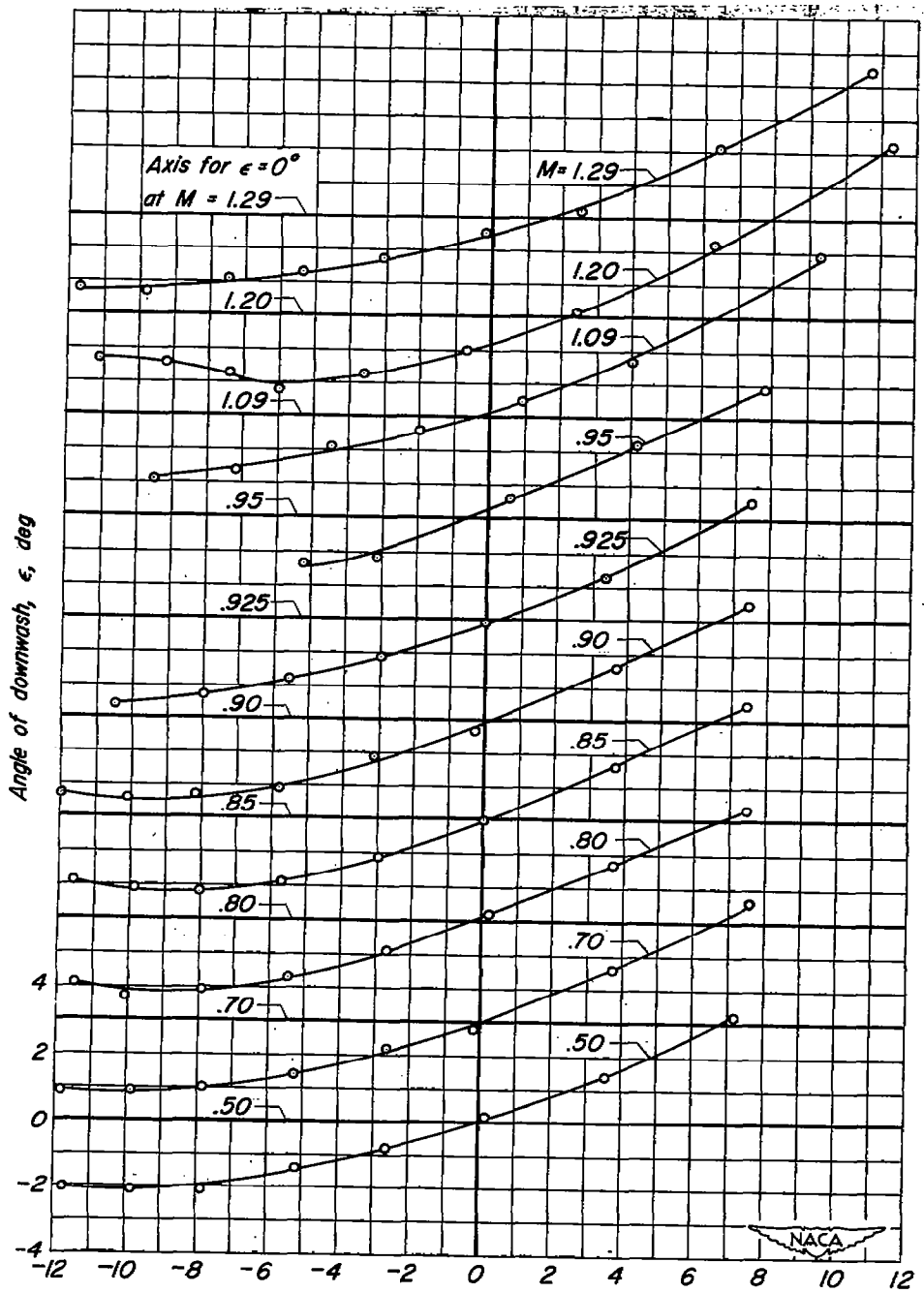

(a) δ_n, 0°; δ_f, 0°.

Figure 4.– Variation of angle of downwash with angle of attack at several Mach numbers; y, 0.25s.

[redacted]

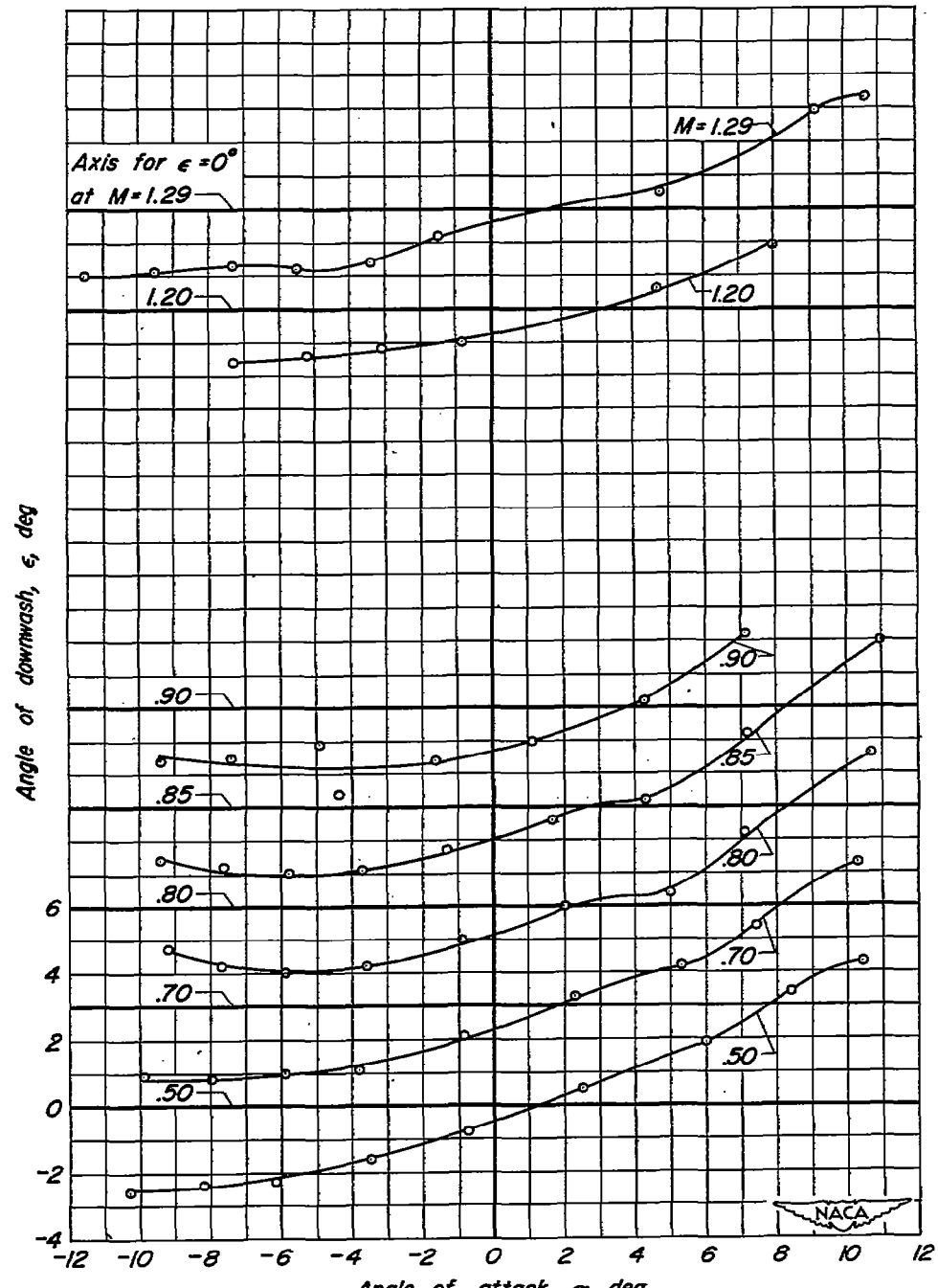

(b) δ_n, -10°; δ_f, 0°.

Figure 4.- Continued.

[redacted]

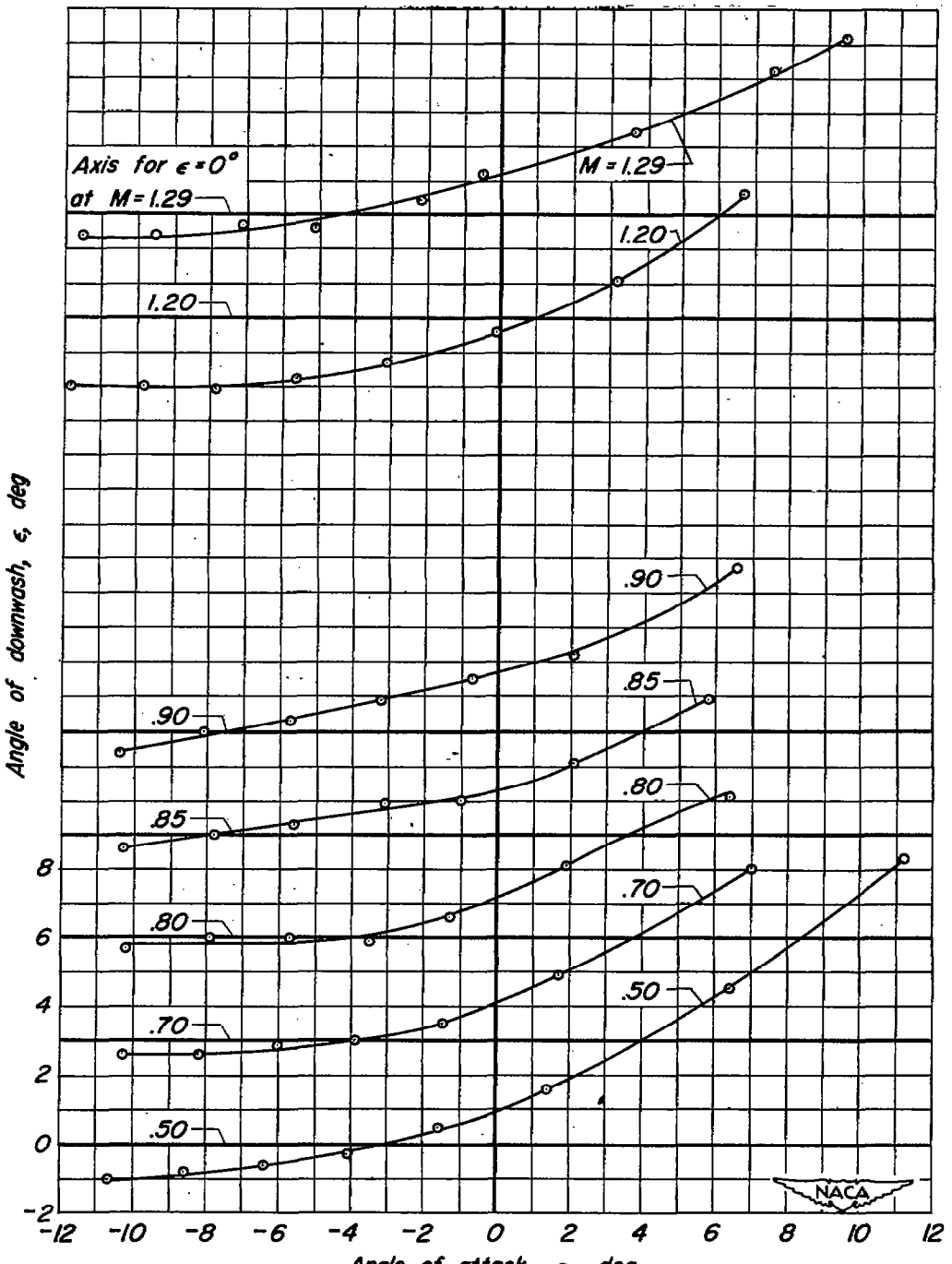

(c) δ_n, 10°; δ_f, 0°.

Figure 4.– Continued.

[redacted]

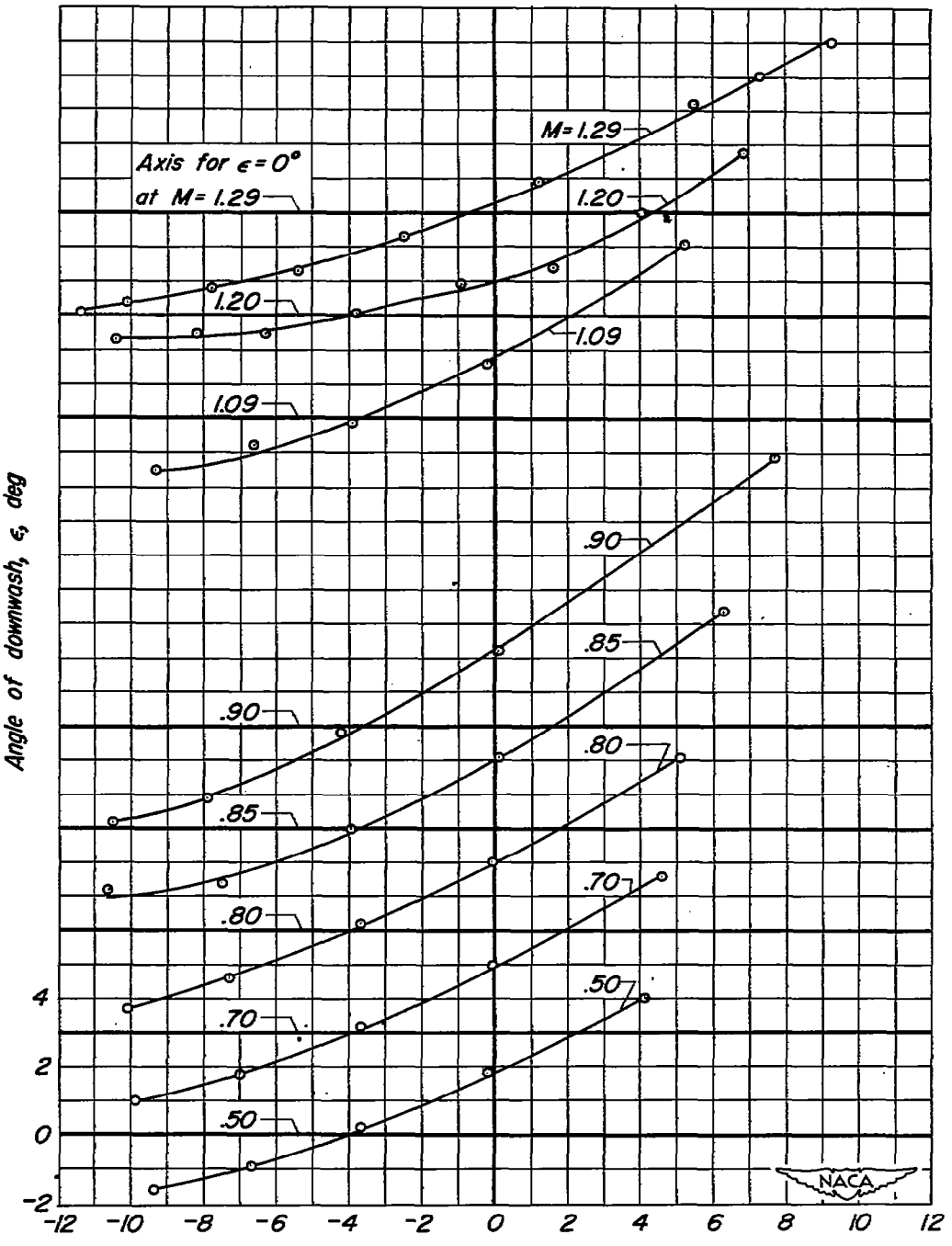

(d) δ_n, 0°; δ_f, 20°.

Figure 4.— Continued.

[redacted]

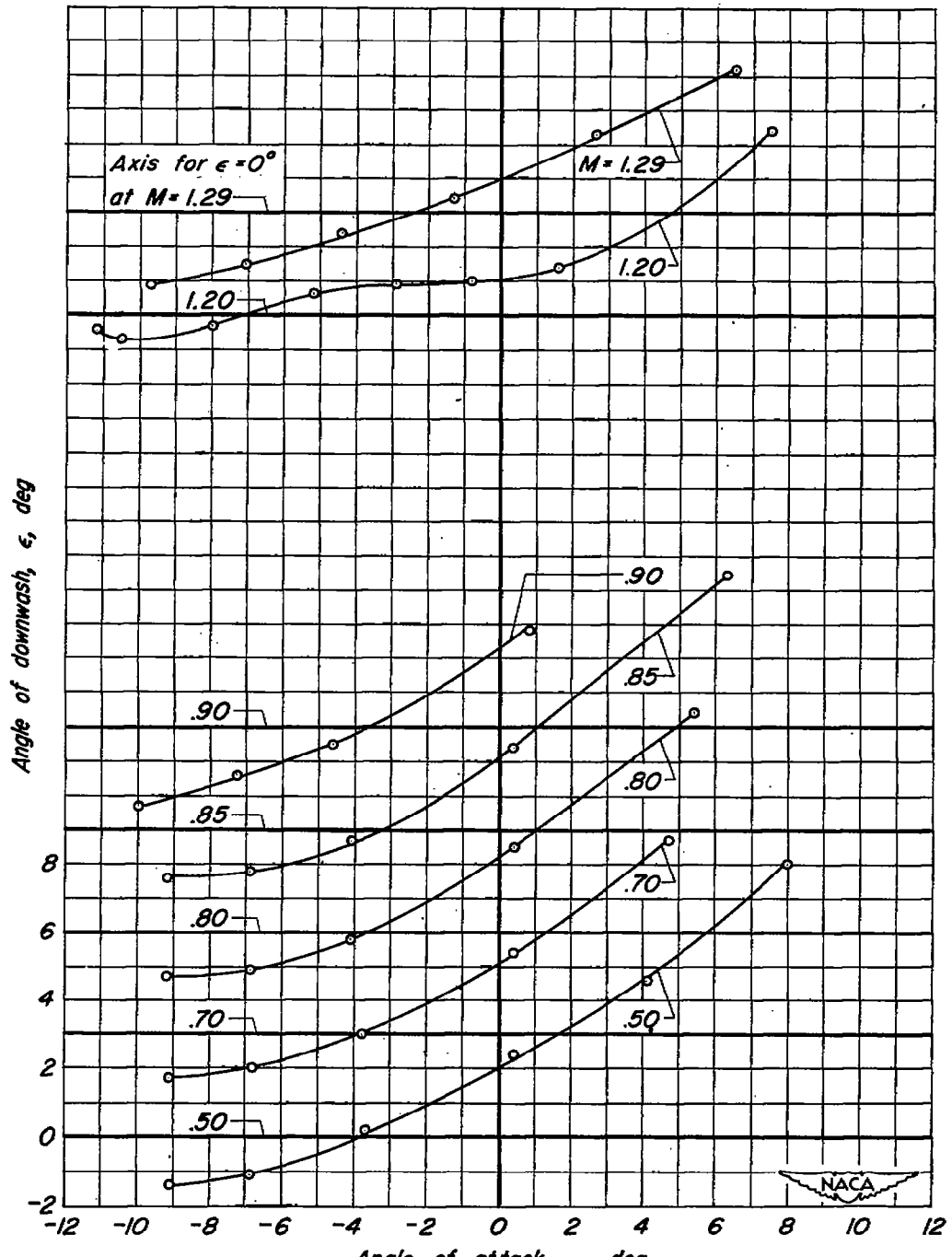

(e) δ_n, 10°; δ_f, 20°.

Figure 4.– Concluded.

[redacted]

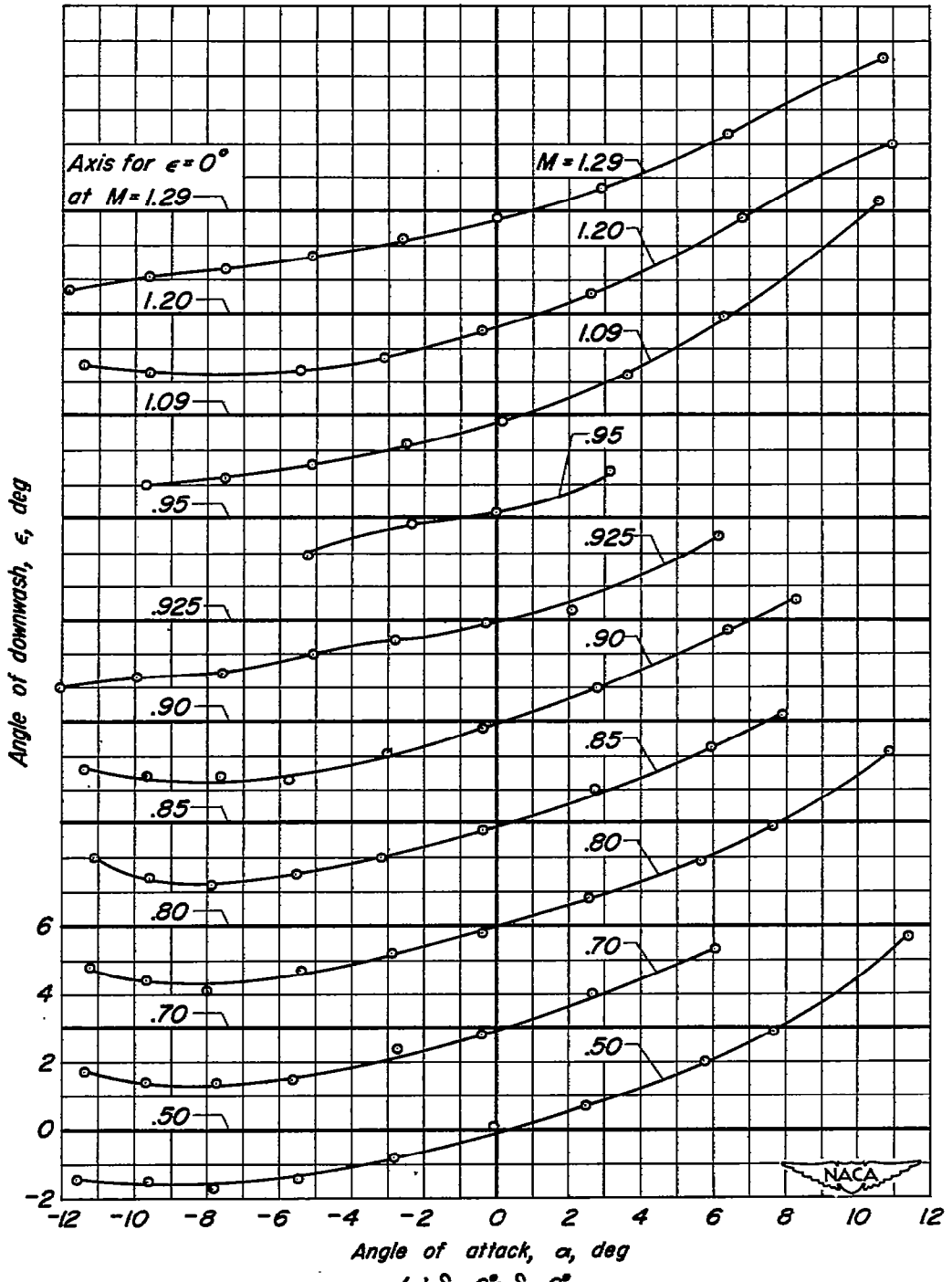

(a) δ_n, 0°; δ_f, 0°.

Figure 5.– Variation of angle of downwash with angle of attack at several Mach numbers; y, 0.50 s.

[redacted]

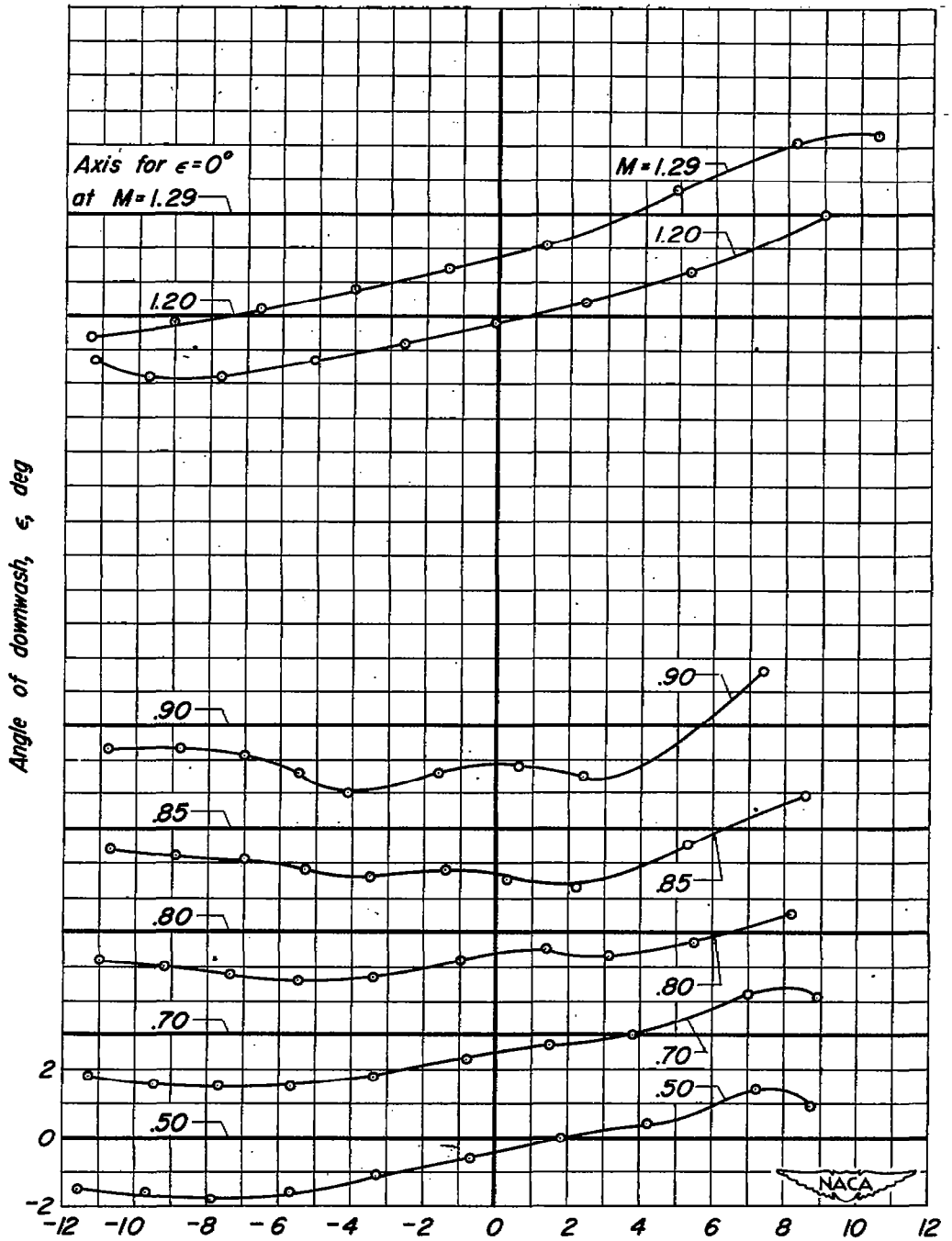

(b) δ_n, -10°; δ_f, 0°.

Figure 5.- Continued.

[redacted]

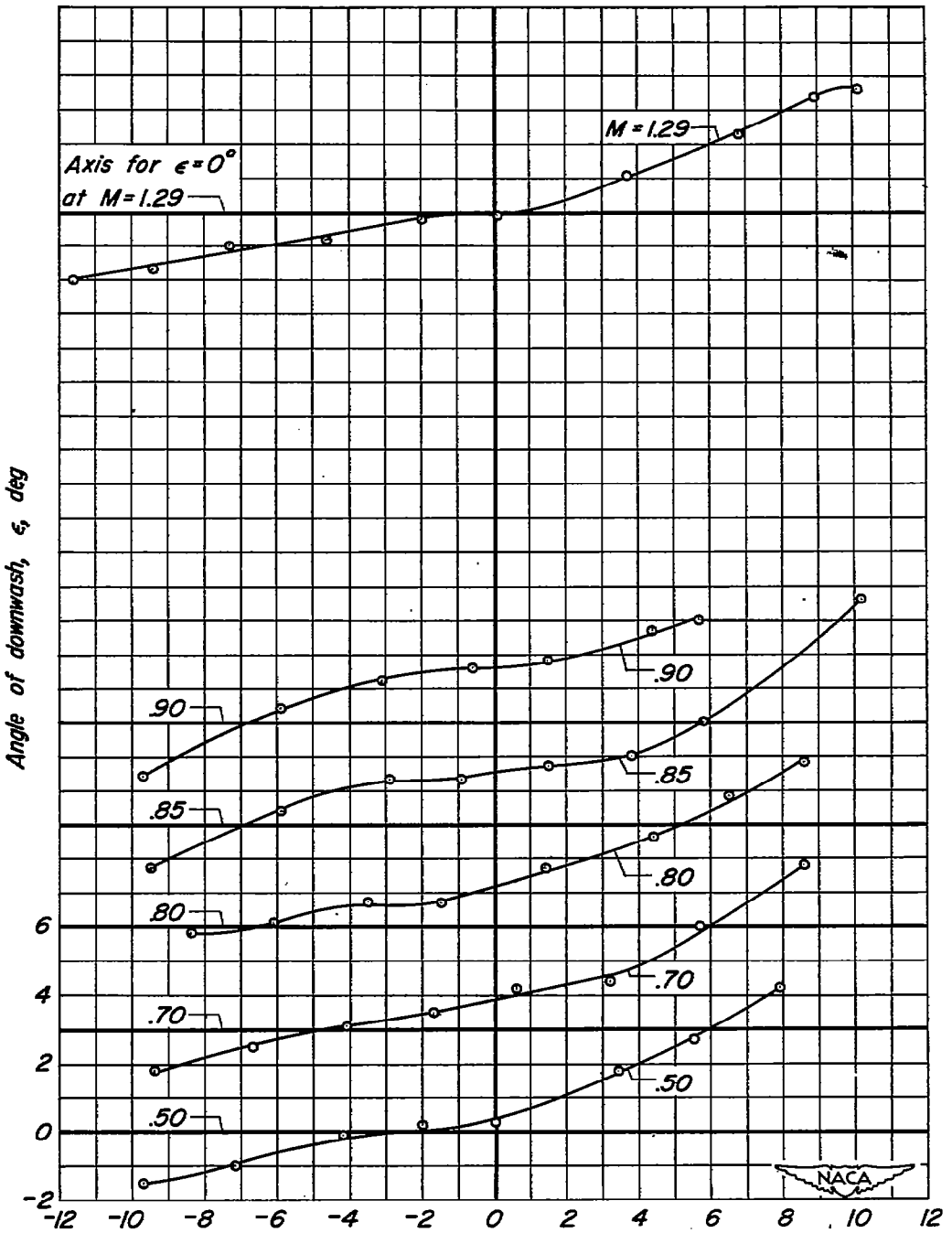

(c) δ_n, 10°; δ_f, 0°.

Figure 5.– Continued.

[redacted]

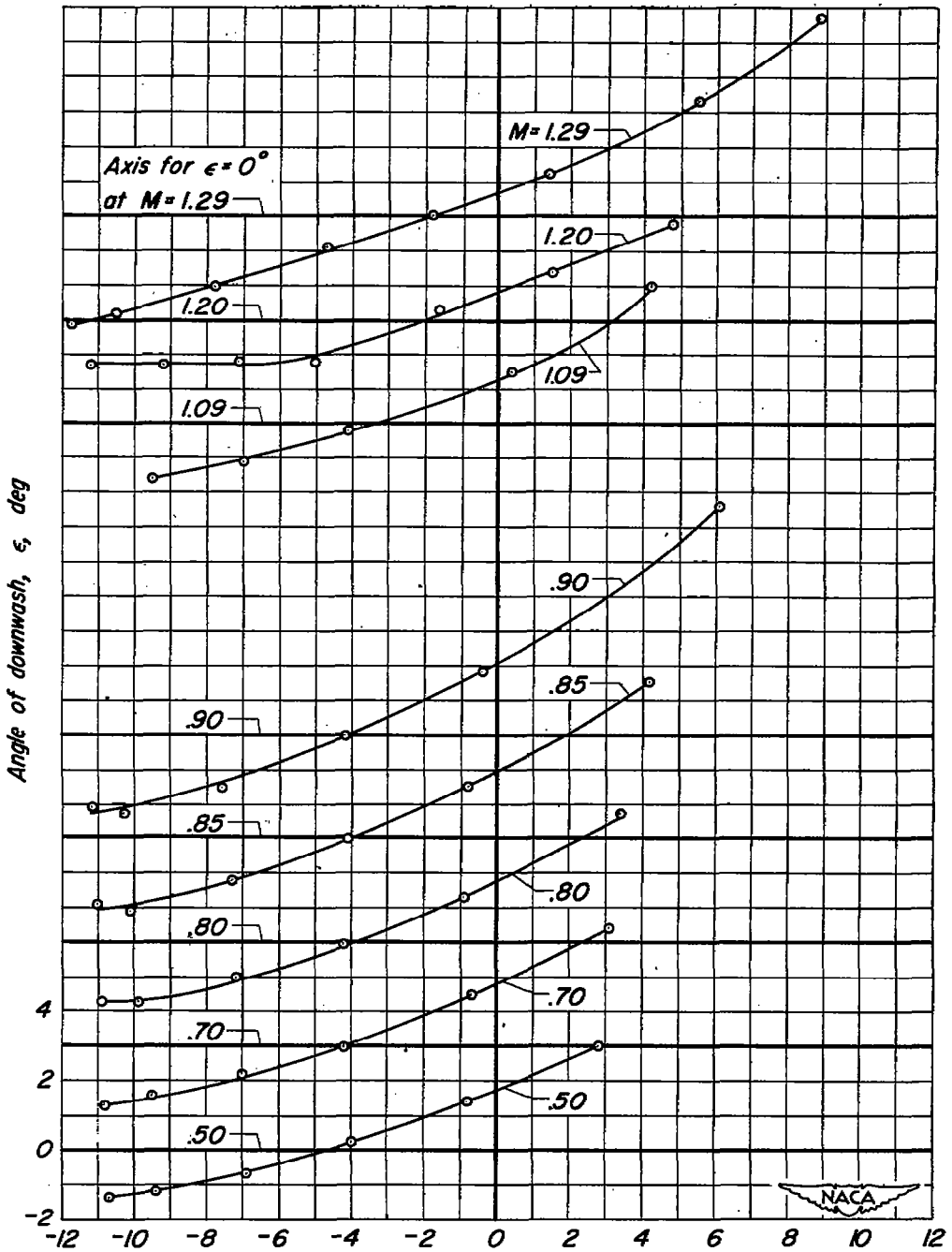

(d) δ_n, 0°; δ_f, 20°.

Figure 5.– Continued.

[redacted]

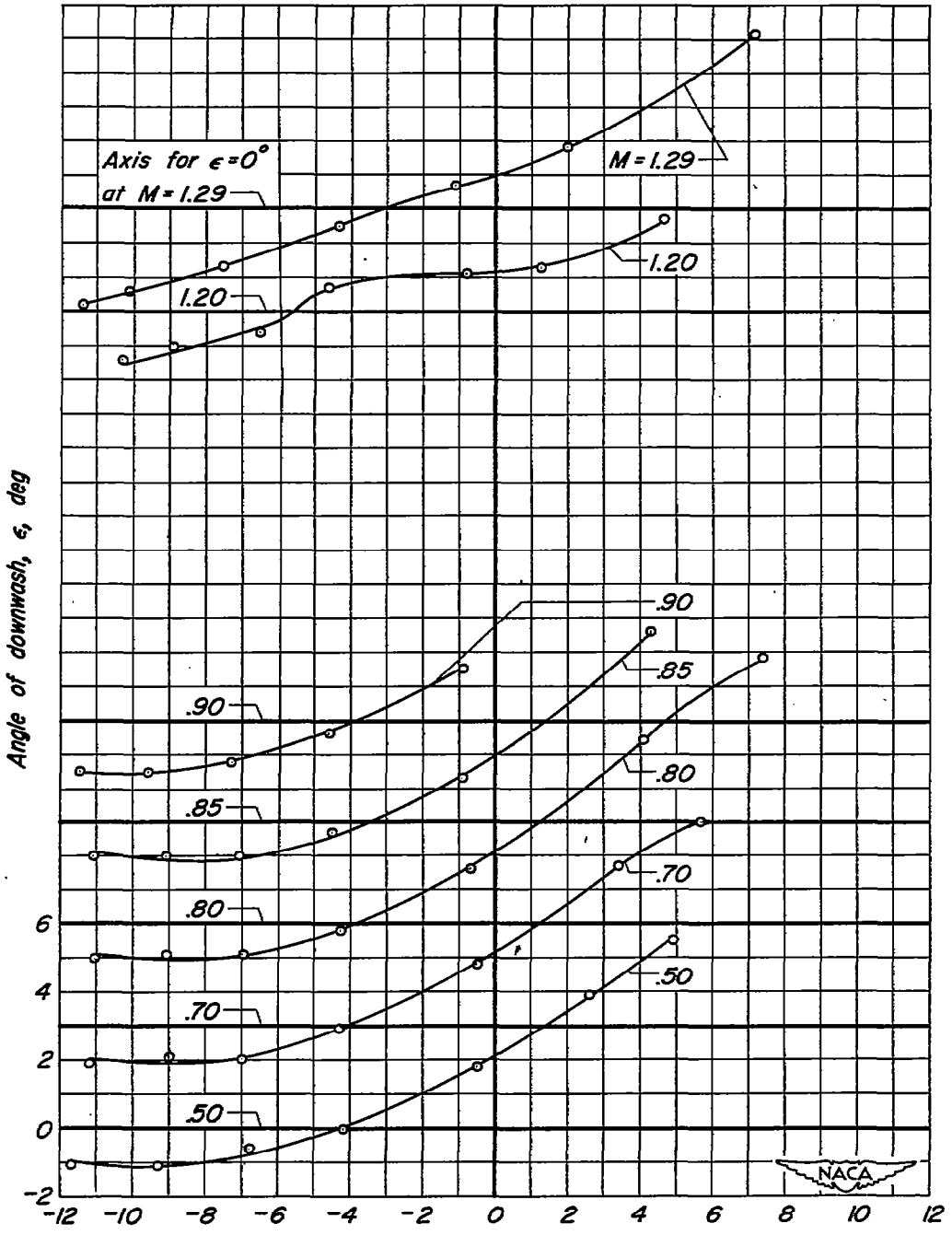

(e) δ_n, 10°; δ_f, 20°.

Figure 5.– Concluded.

[redacted]

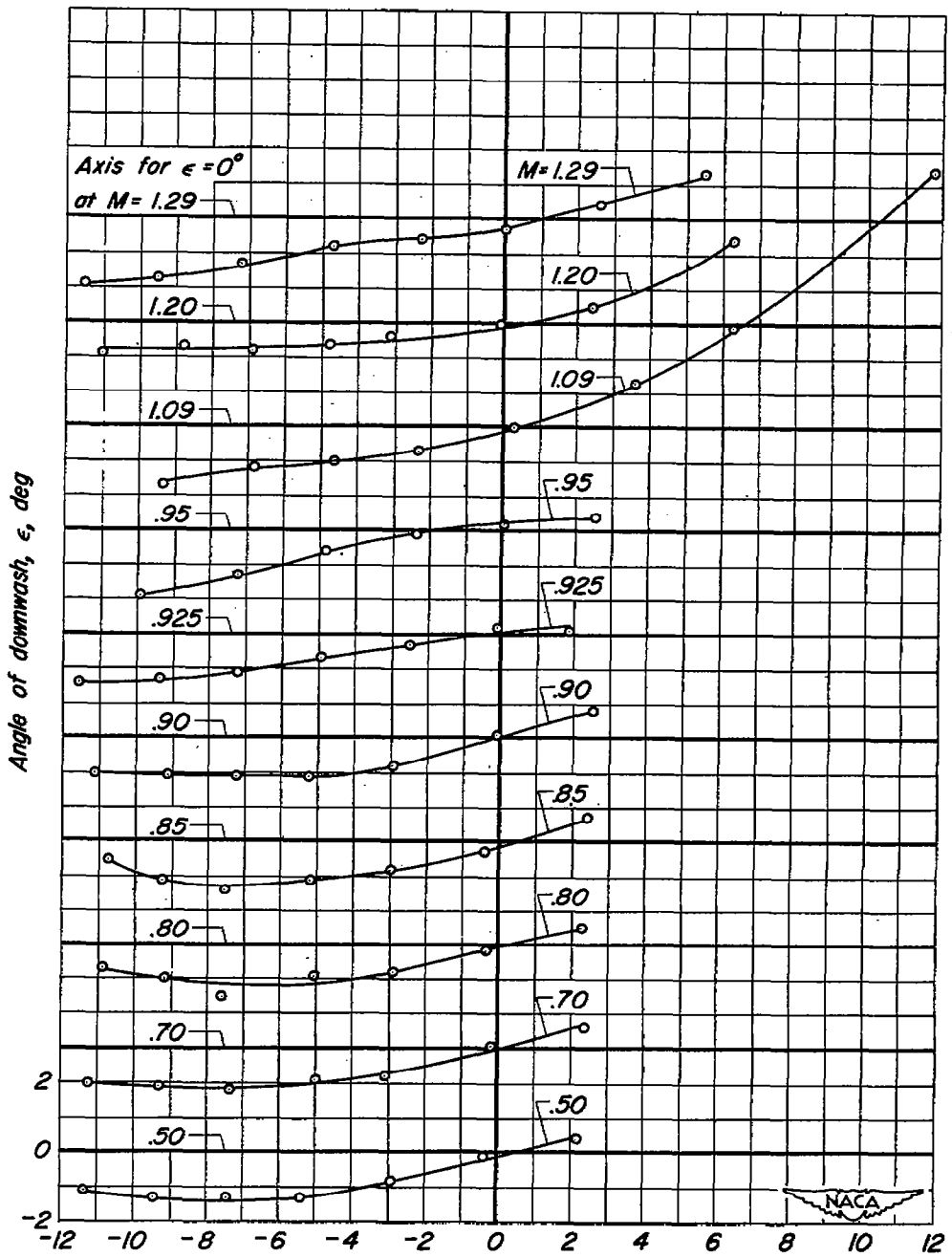

(a) δ_n, 0°; δ_f, 0°.

Figure 6.– Variation of angle of downwash with angle of attack at several Mach numbers; y, 0.625 s.

[redacted]

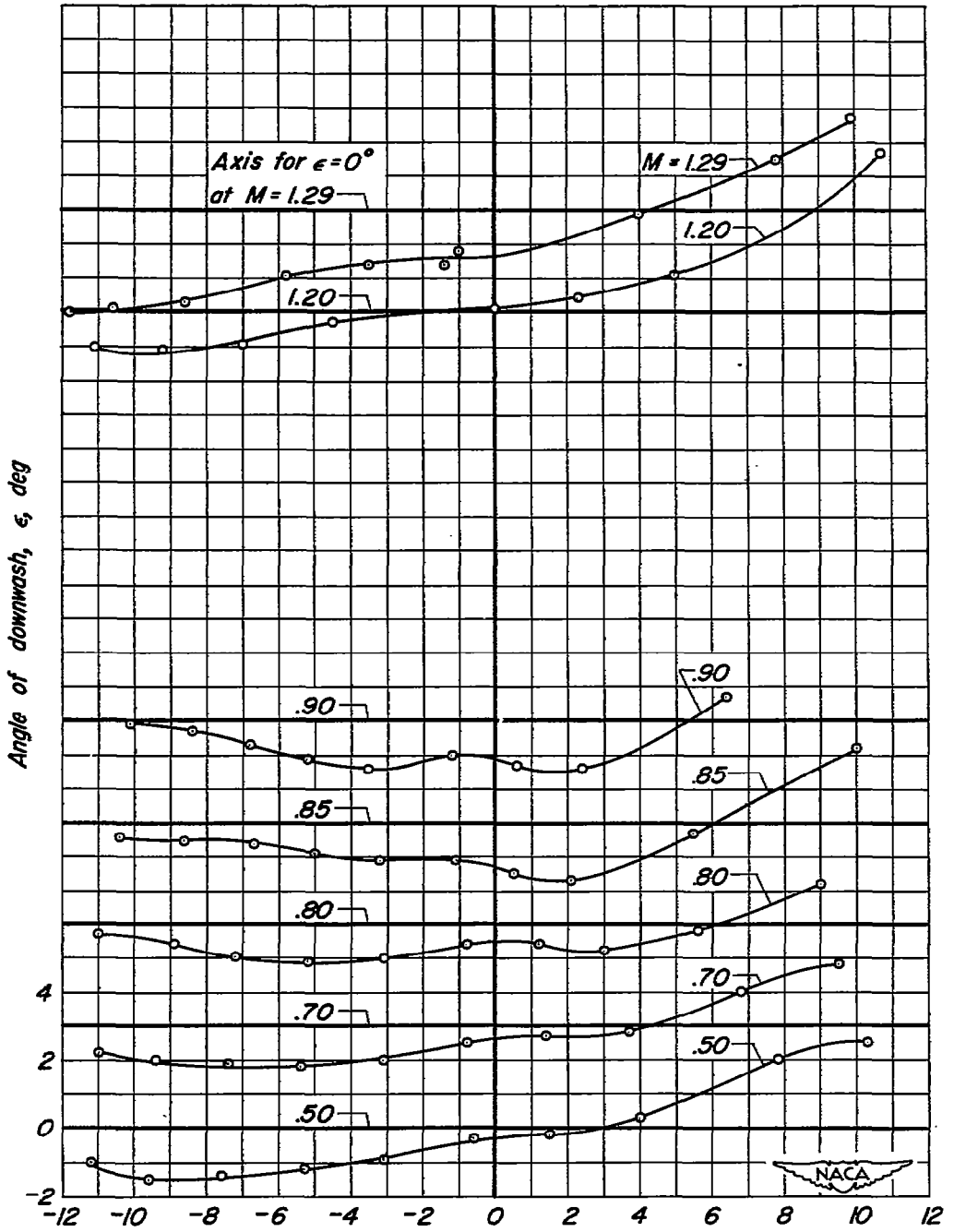

(b) δ_n, -10°; δ_f, 0°.

Figure 6.- Continued.

[redacted]

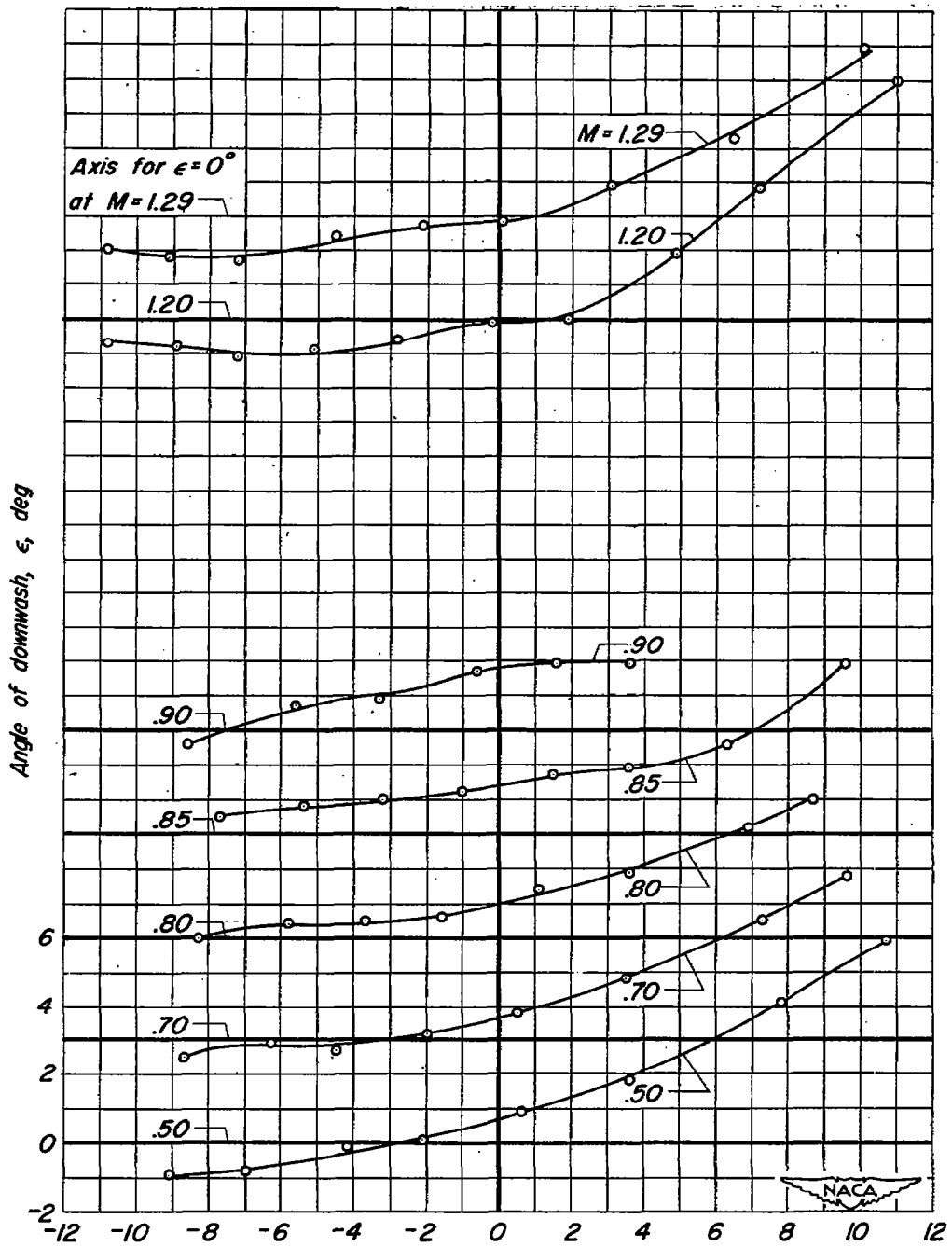

(c) δ_n, 10°; δ_f, 0°.

Figure 6.– Continued.

[redacted]

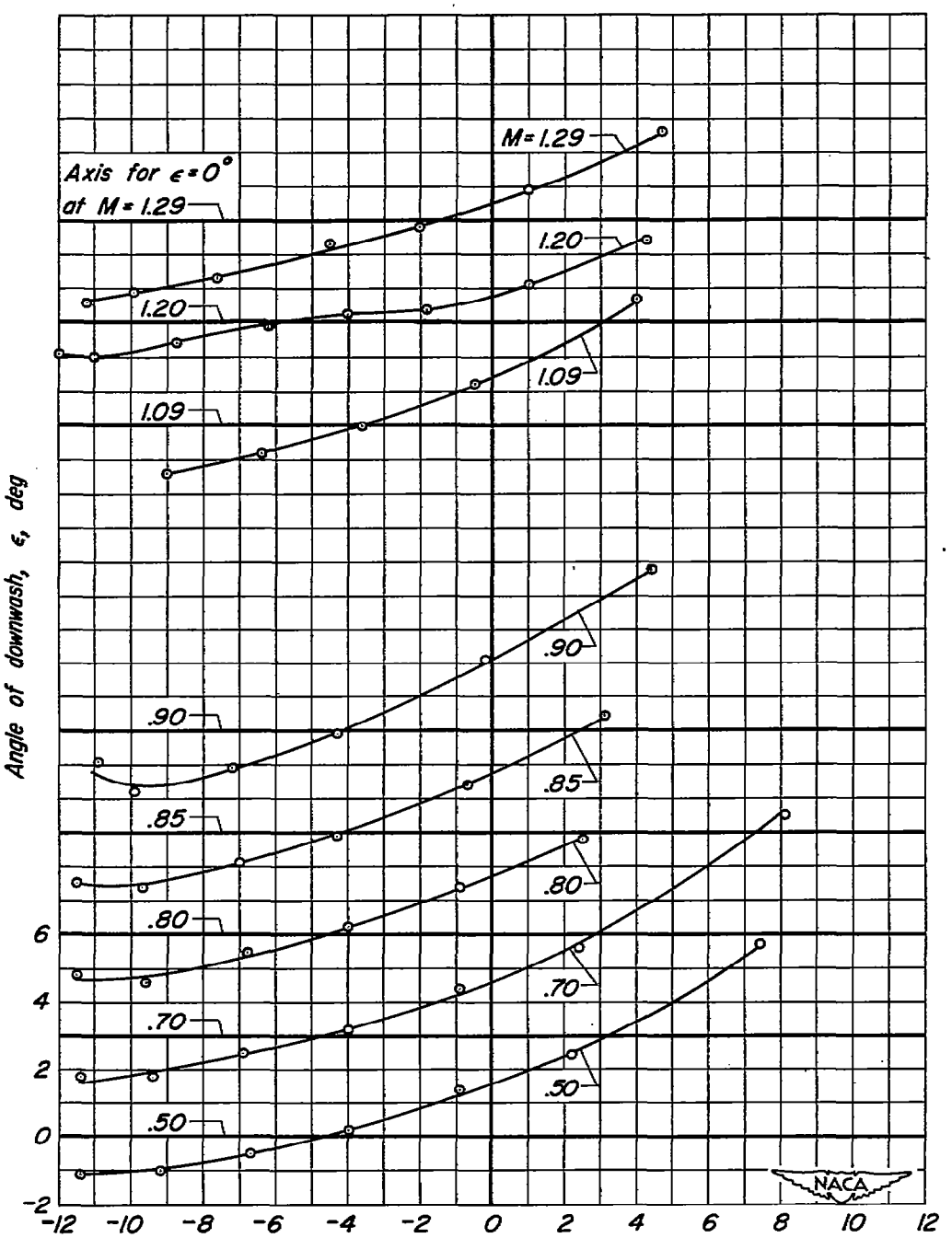

(d) δ_n, 0°; δ_f, 20°.

Figure 6.— Continued.

[redacted]

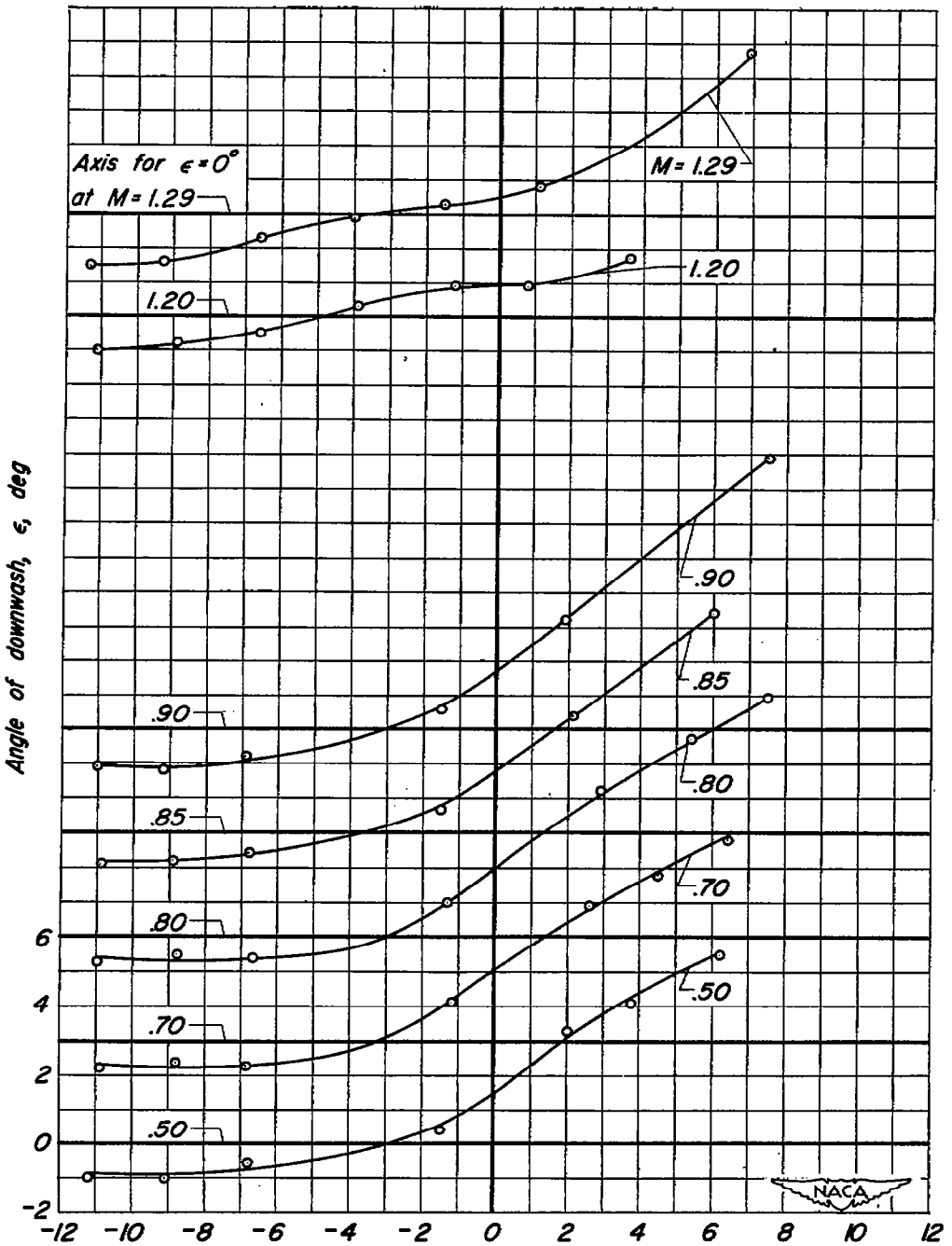

(e) δ_n, 10°; δ_f, 20°.

Figure 6.– Concluded.

[redacted]

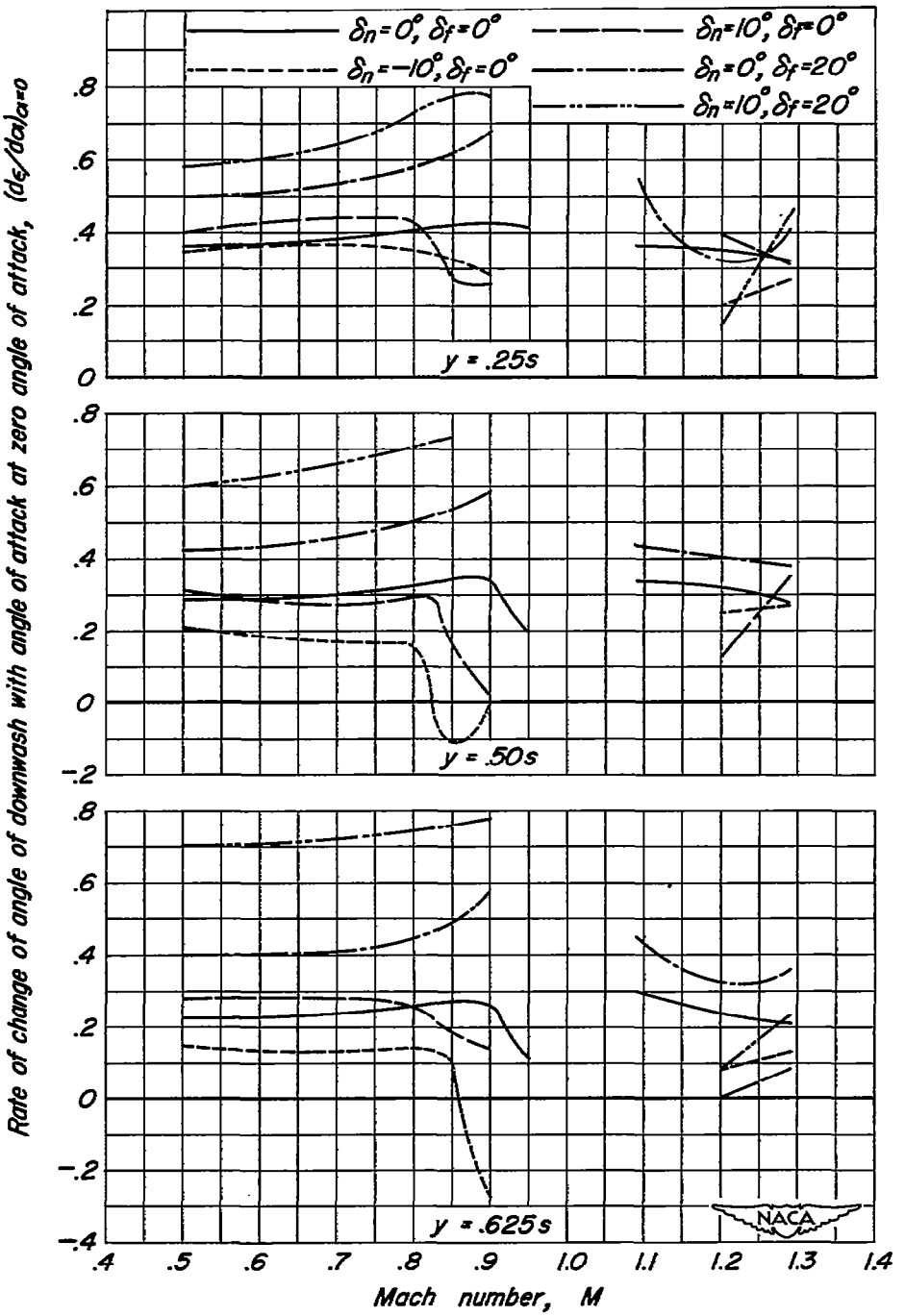

Figure 7.— Variation with Mach number of rate of change of angle of downwash with angle of attack at zero angle of attack for several spanwise stations.

[redacted]

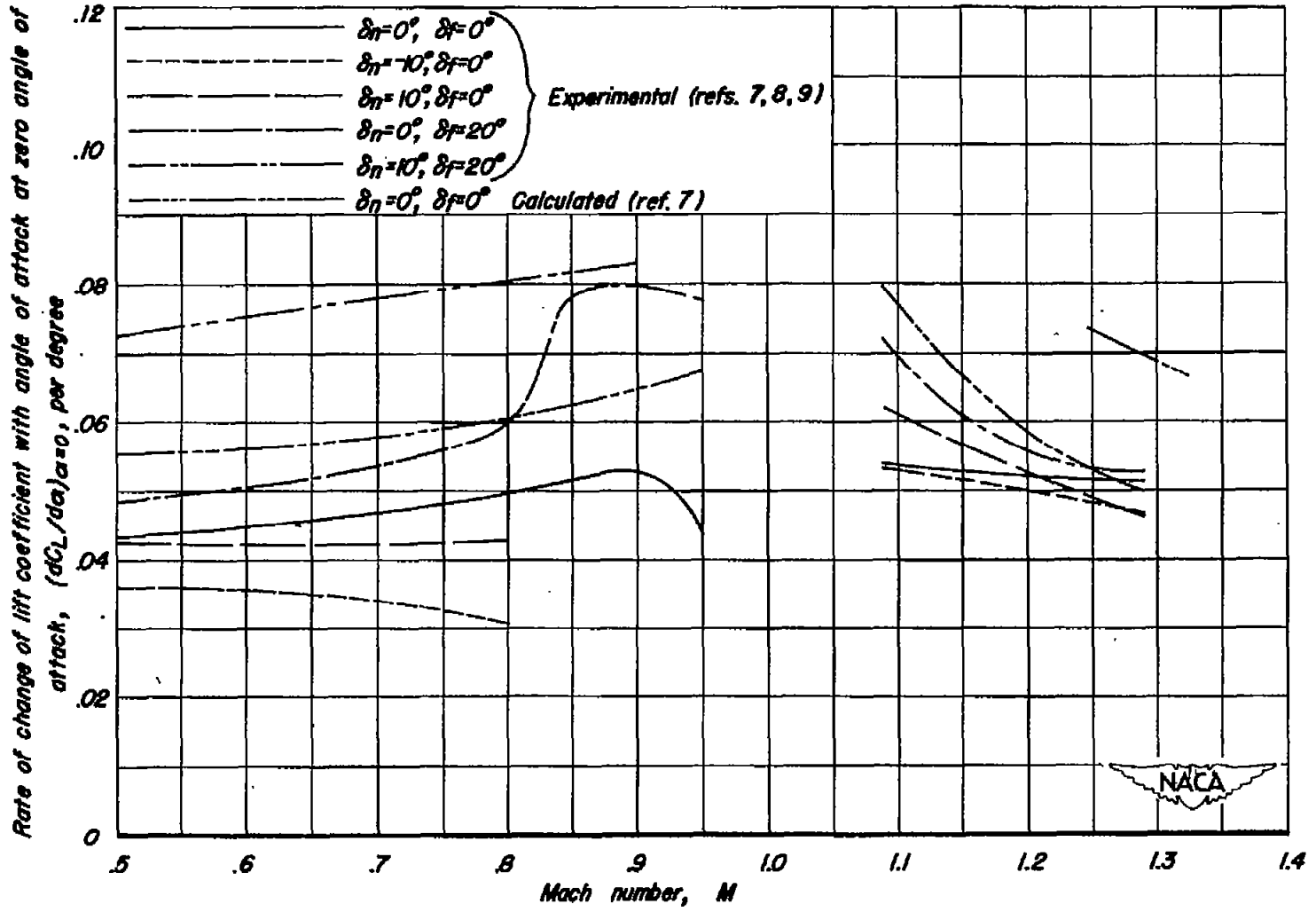

Figure 8.– Variation with Mach number of rate of change of lift coefficient with angle of attack at zero angle of attack.

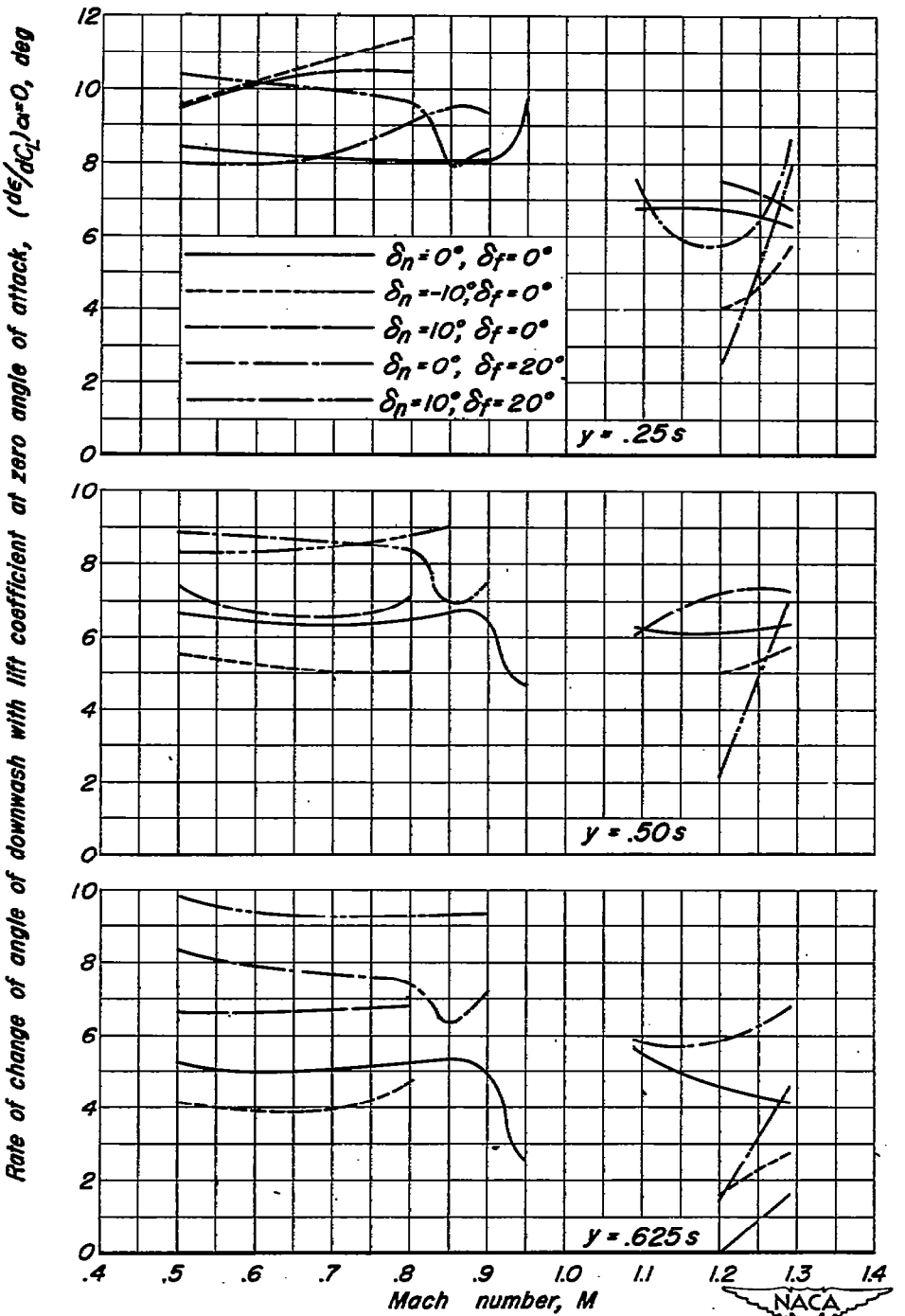

Figure 9.— Variation with Mach number of rate of change of angle of downwash with lift coefficient at zero angle of attack for several spanwise stations.

[redacted]

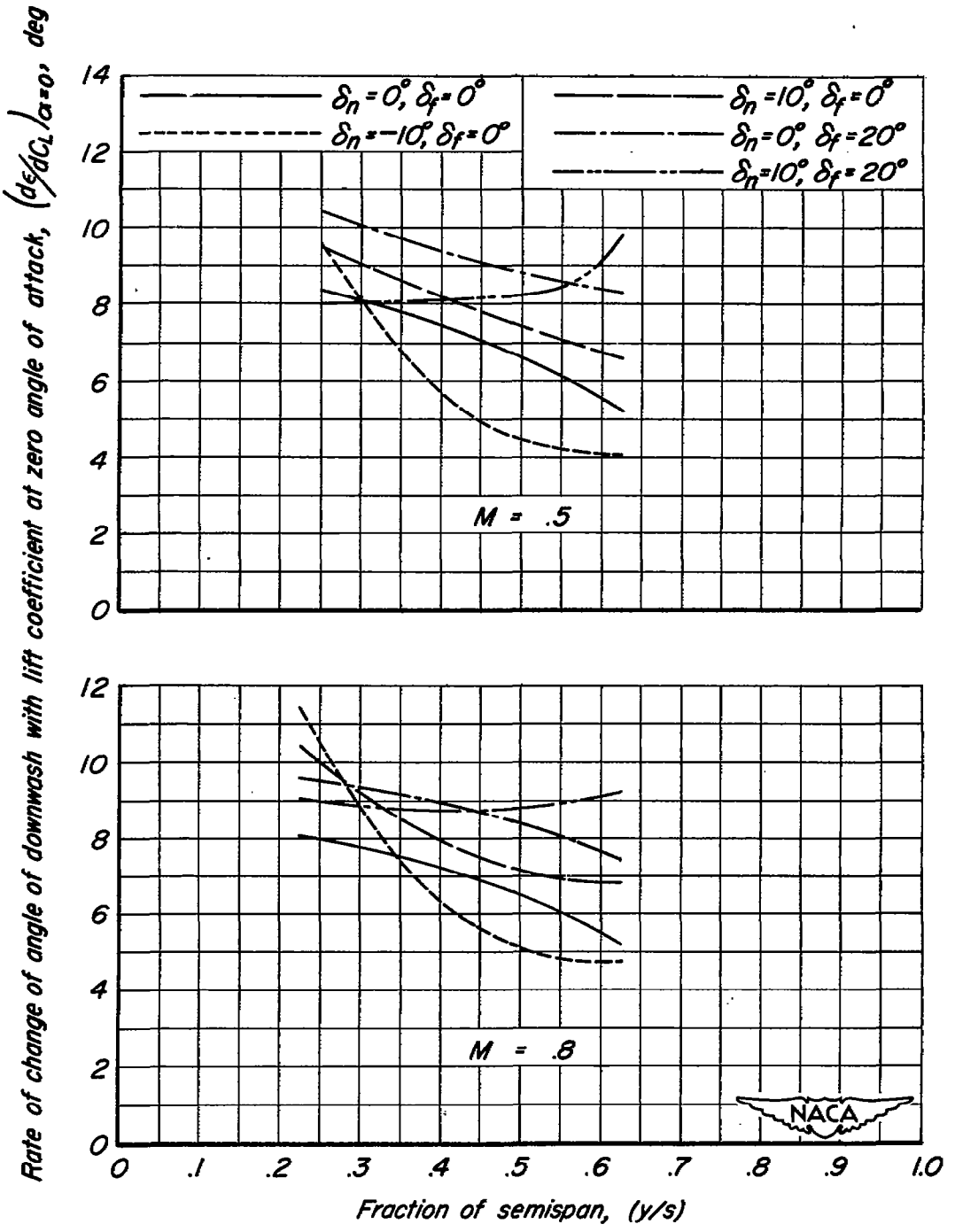

Figure 10.— Spanwise variation of rate of change of angle of downwash with lift coefficient at zero angle of attack for Mach numbers of 0.5 and 0.8.

[redacted]

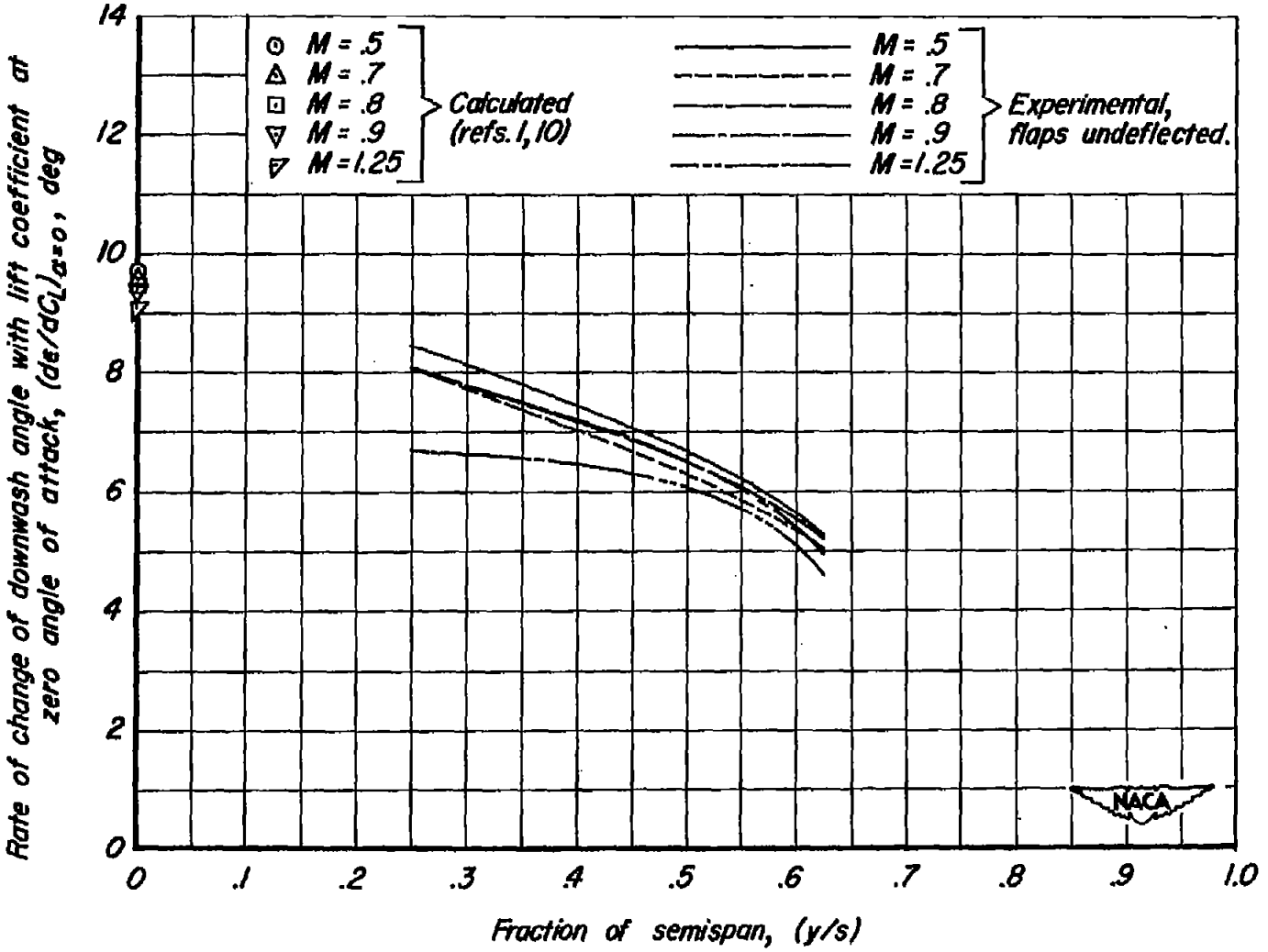

Figure 11.– Variation with spanwise location of rate of change of downwash angle with lift coefficient at zero angle of attack for several Mach numbers; flaps undeflected.

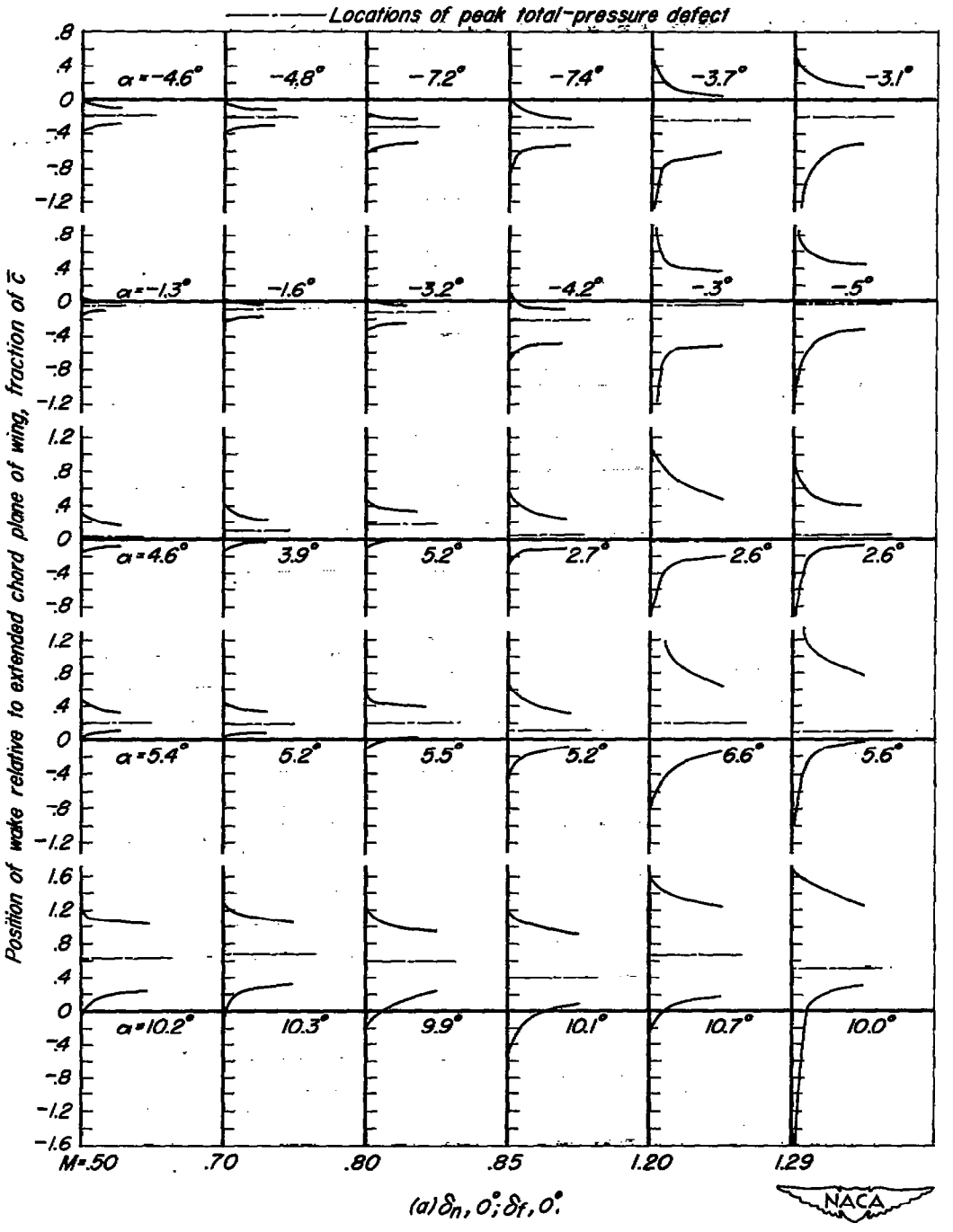

Figure 12.– Variation with Mach number and angle of attack of position of wake relative to extended chord plane of wing. Wake survey rake located 4.74 c̄ downstream from midchord line of wing.

[redacted]

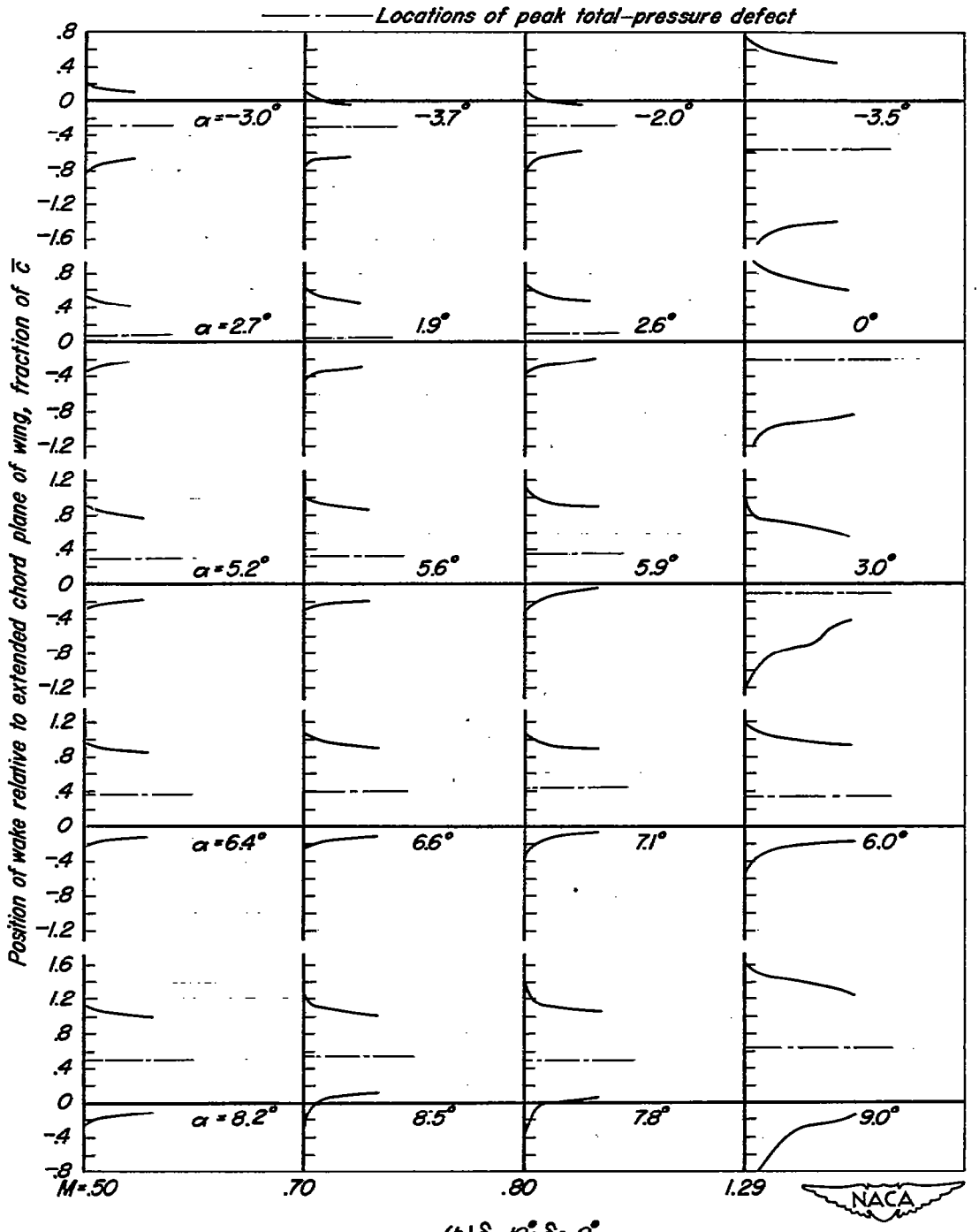

(b) δ_n, 10°; δ_f, 0°.

Figure 12.— Continued.

[redacted]

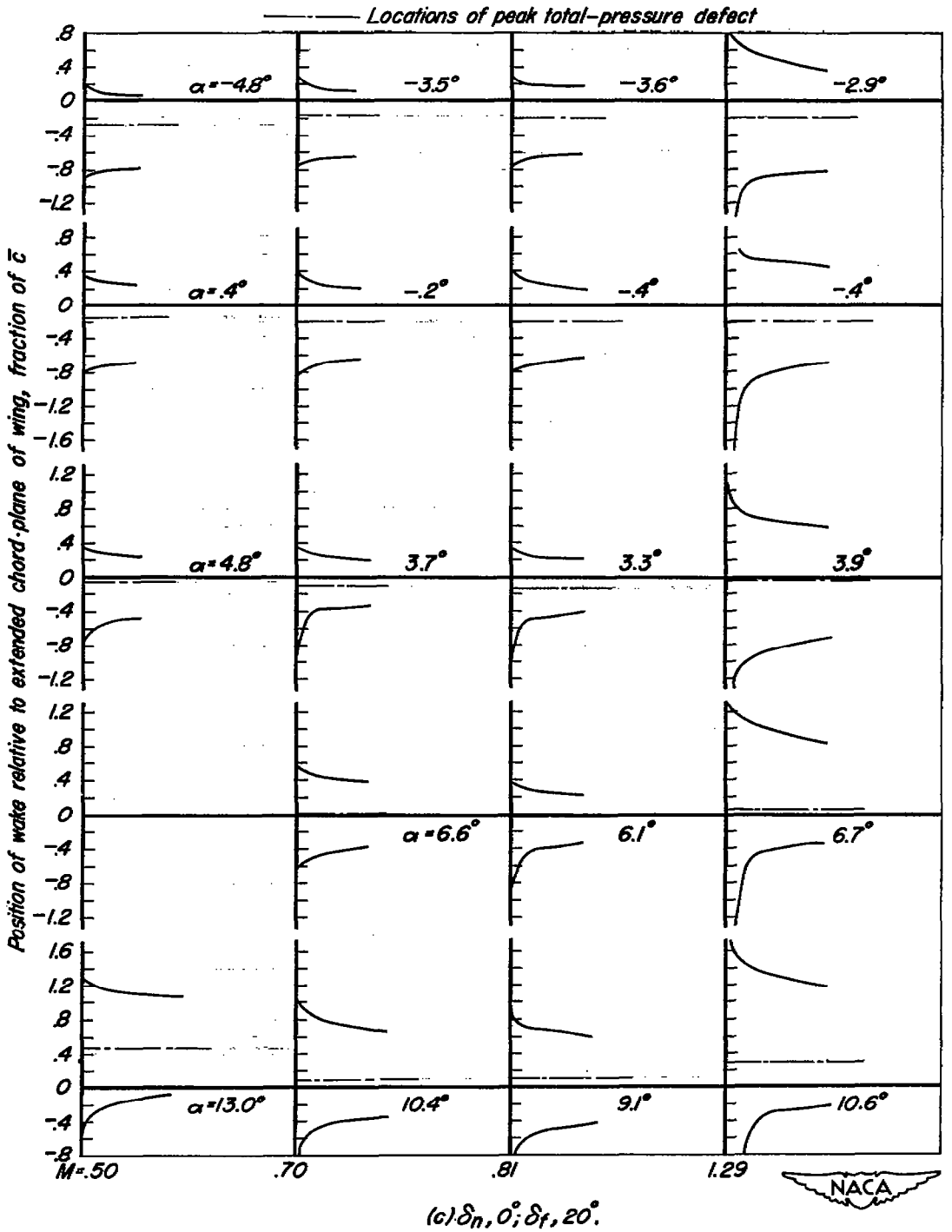

(c) δ_n, 0°; δ_f, 20°.

Figure 12.– Continued.

[redacted]

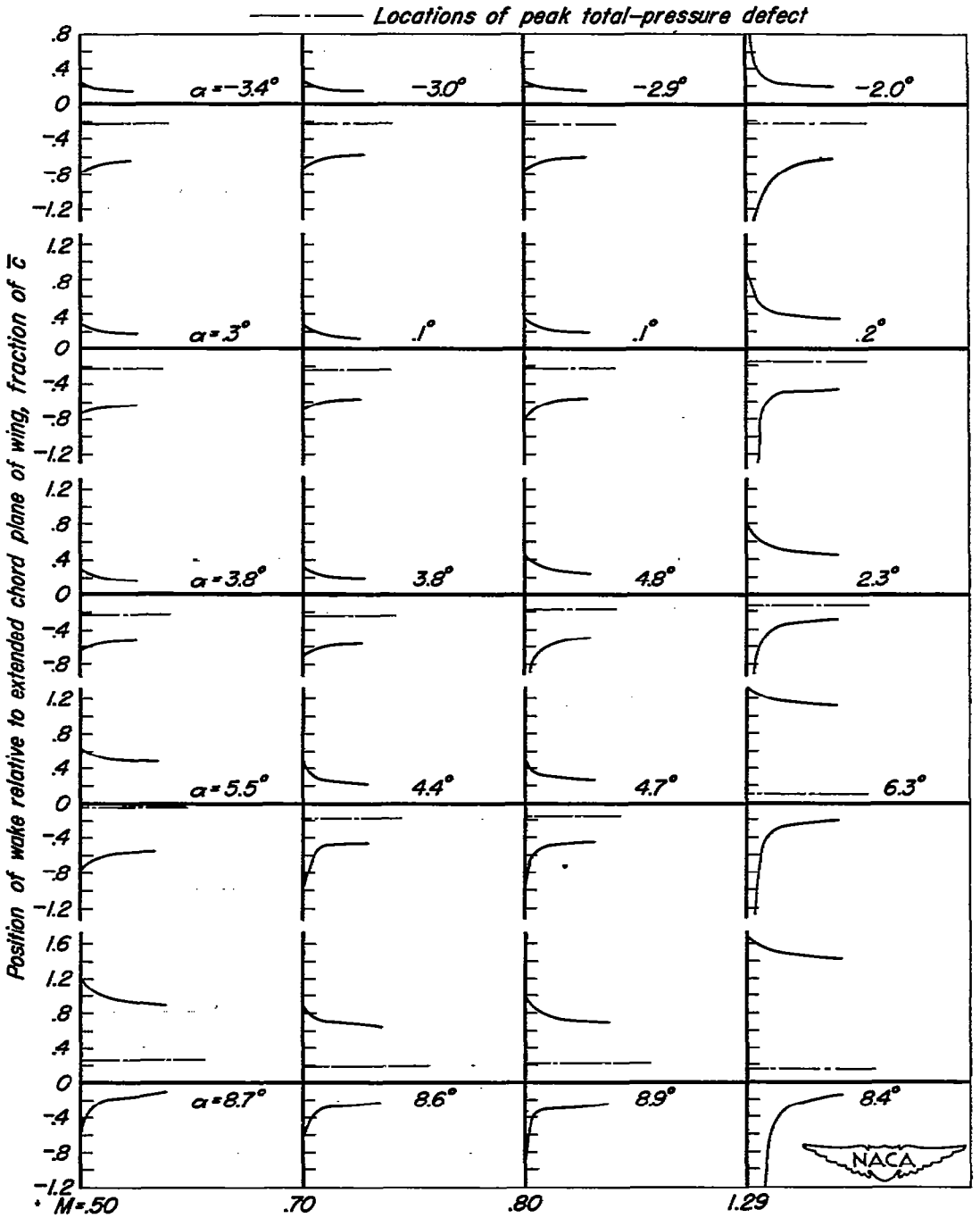

(d) δ_n, 10°; δ_f, 20°.

Figure 12.– Continued.

[redacted]

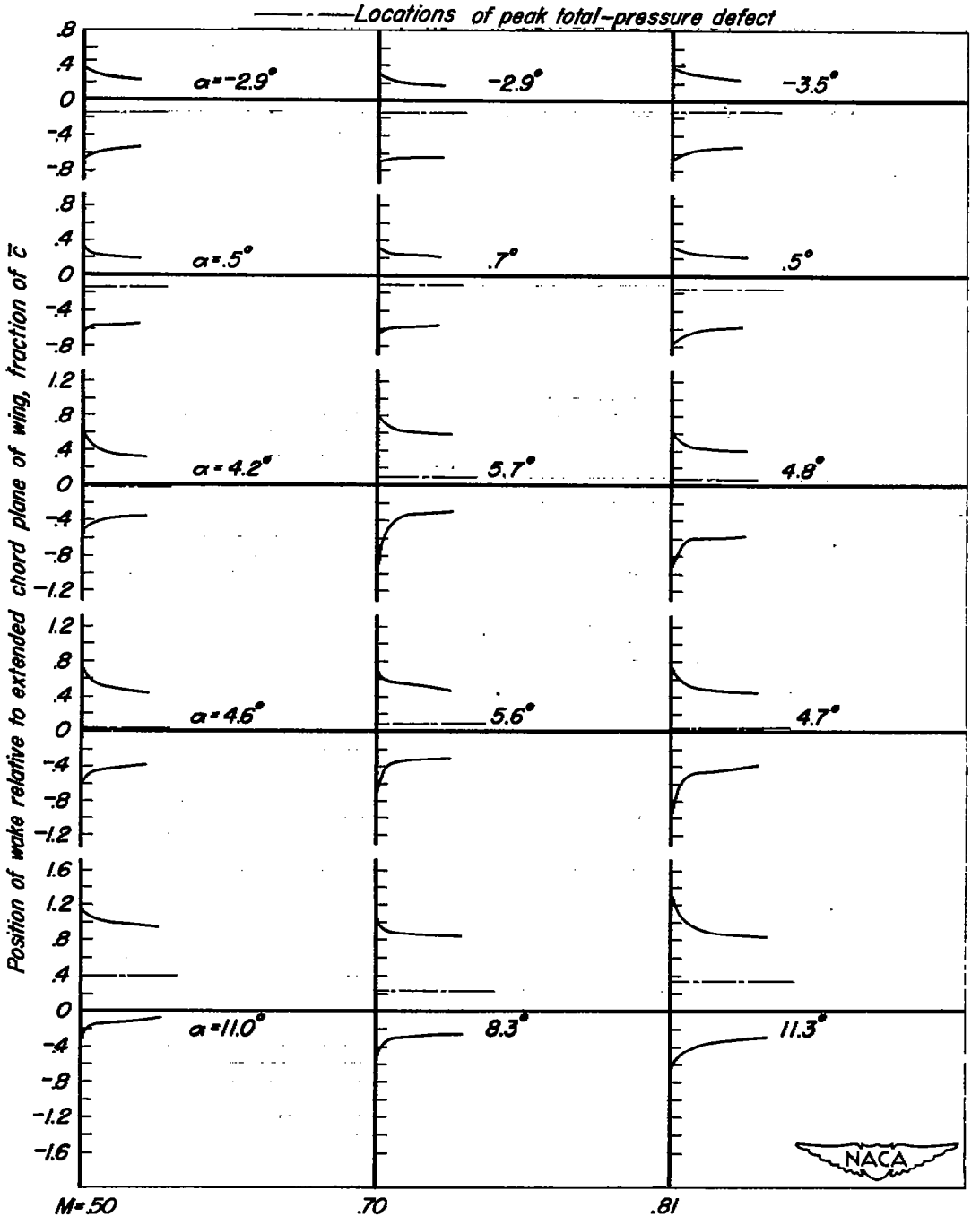

(e) δ_n, -10°; δ_f, 20°.

Figure 12.- Continued.

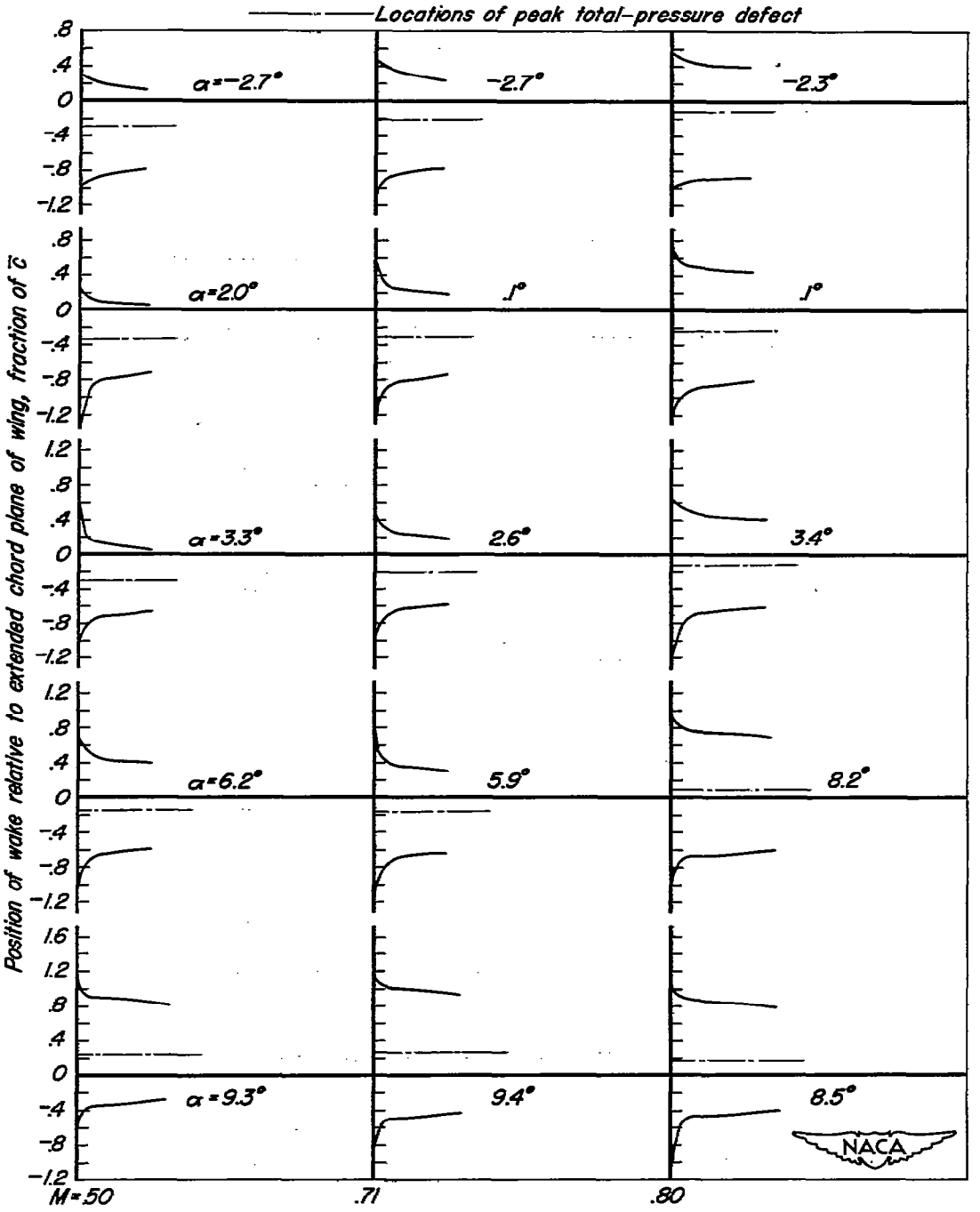

(f) δ_n,-20°; δ_f,40°.

Figure 12.- Concluded.

[redacted]

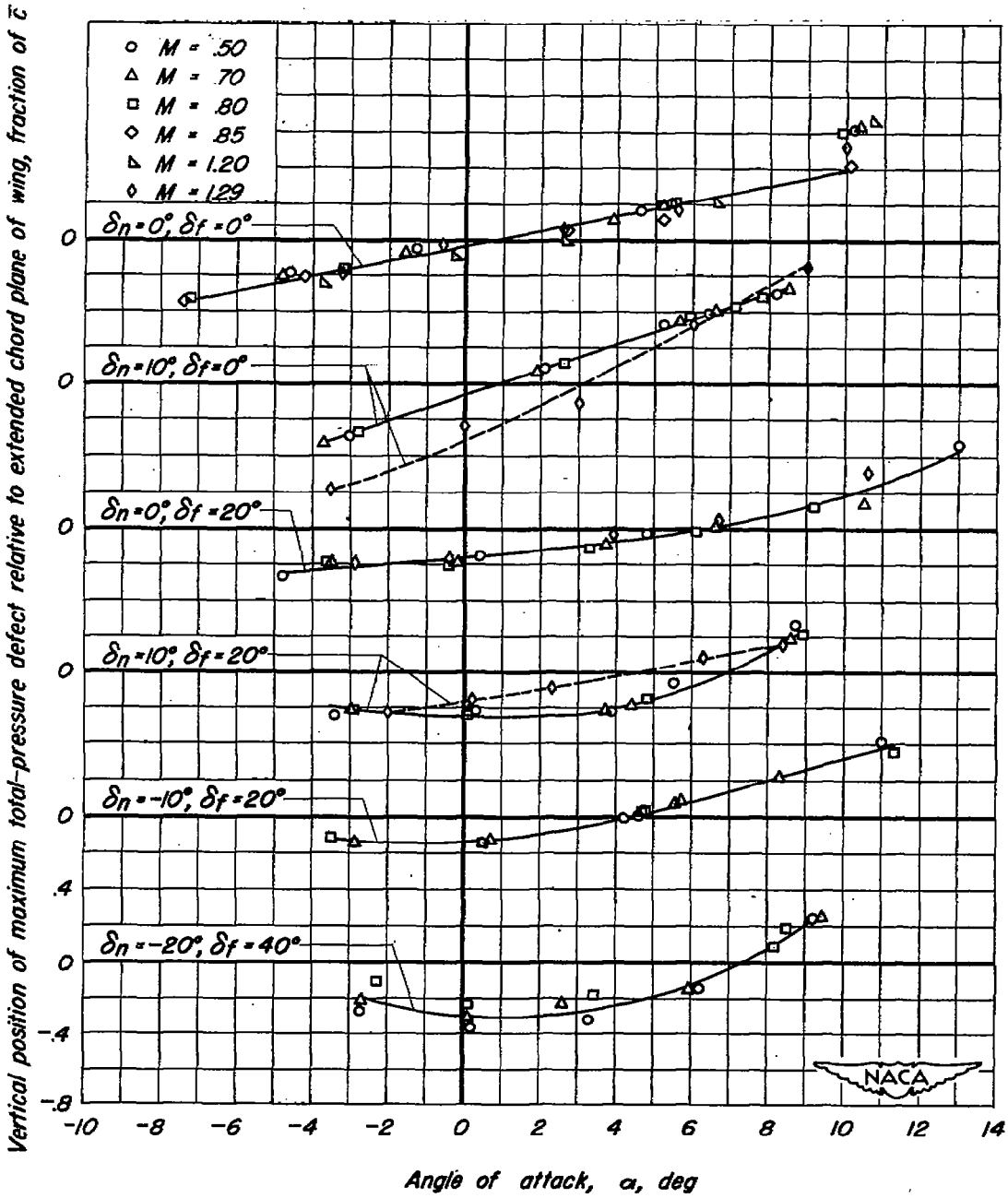

Figure 13.– Variation with angle of attack of vertical location of maximum total-pressure defect relative to extended chord plane of wing for various Mach numbers and combinations of flap deflections.

[redacted]

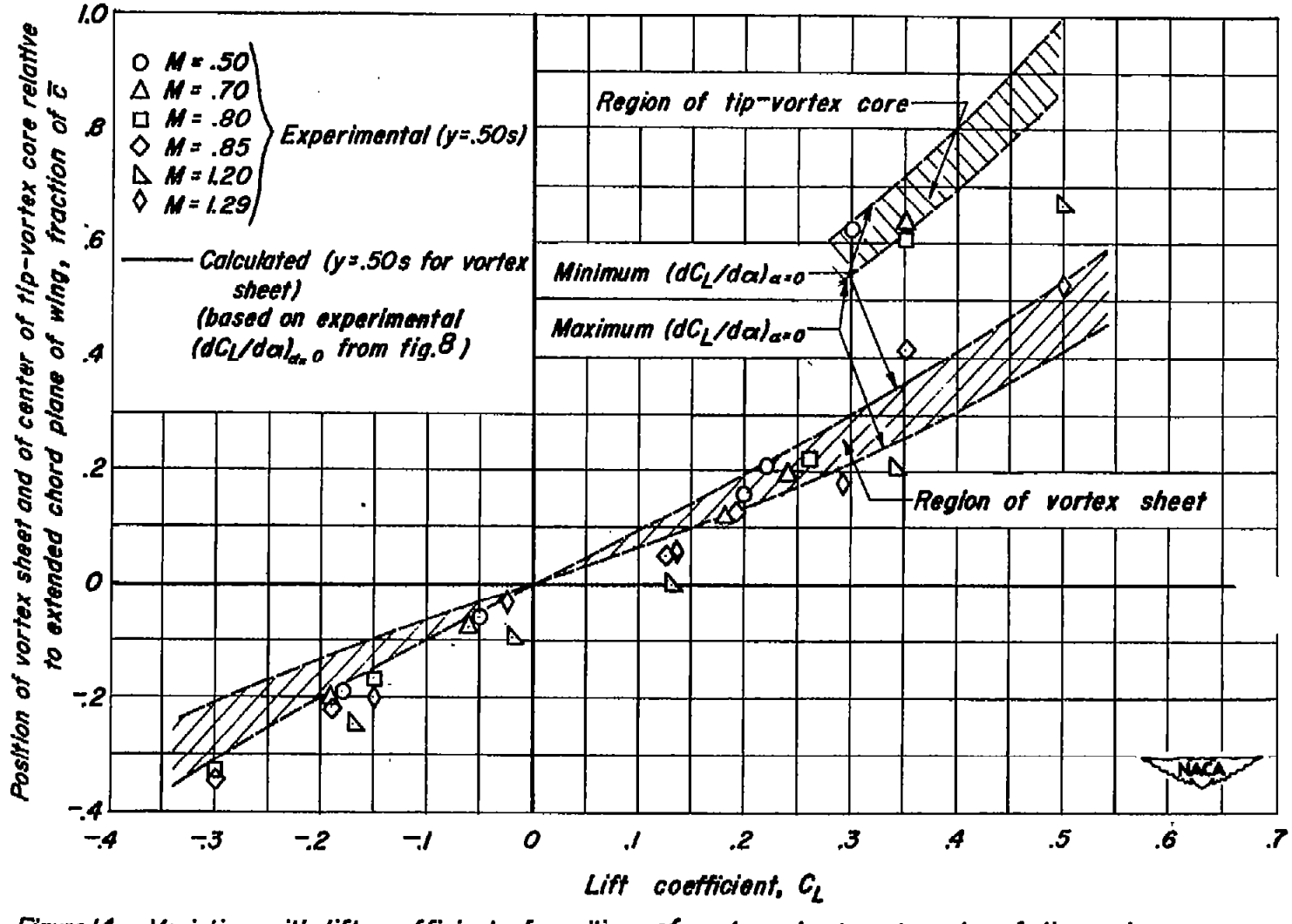

Figure 14.— Variation with lift coefficient of positions of vortex sheet and center of tip-vortex core relative to extended chord plane of wing at various Mach numbers; flaps undeflected.